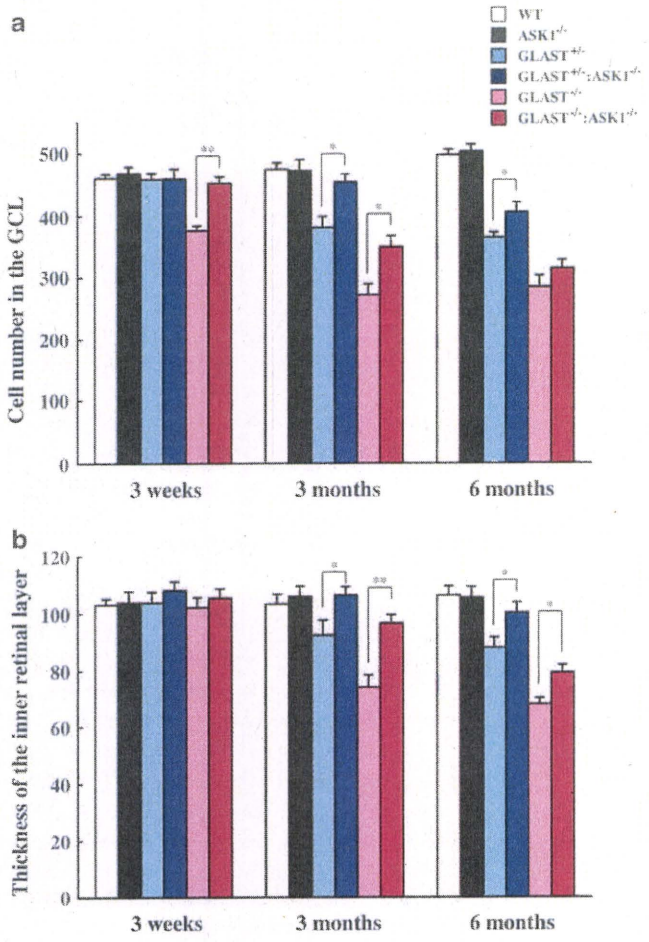

Figure 3 Quantification of the severity of glaucoma. (**a**) RGC number in WT, ASK1$^{-/-}$, GLAST$^{+/-}$, GLAST$^{+/-}$:ASK1$^{-/-}$, GLAST$^{-/-}$ and GLAST$^{-/-}$:ASK1$^{-/-}$ mice. The number of neurons in the GCL was counted in retinal sections from one ora serrata through the optic nerve to the other ora serrata. (**b**) Thickness of the inner retinal layer in WT, ASK1$^{-/-}$, GLAST$^{+/-}$, GLAST$^{+/-}$:ASK1$^{-/-}$, GLAST$^{-/-}$ and GLAST$^{-/-}$:ASK1$^{-/-}$ mice. $^{**}P<0.01$, $^{*}P<0.05$

GLAST$^{+/-}$ mice ($P<0.05$) and in normal range compared with WT mice ($P=0.94$, Figure 4m). Similarly, RGC number in GLAST$^{-/-}$:ASK1$^{-/-}$ mice (3392 ± 102; $n=3$) was increased compared with GLAST$^{-/-}$ mice (2592 ± 269; $n=3$) ($P<0.05$,Figure 4m).

Degeneration of the optic nerve is one of the hallmarks of glaucoma. To analyze morphological changes in the optic nerve, semi-thin transverse sections were cut and stained with toluidine blue (Figure 4i–l). Consistent with severe RGC loss, the degenerating axons in 3 M GLAST$^{+/-}$ mice had abnormally dark axonal profiles (arrowheads in Figure 4k). Such degenerating axons, however, were almost absent in GLAST$^{+/-}$:ASK1$^{-/-}$ mice (Figure 4l). Taken together, these results demonstrate that ASK1 deficiency protects against RGC loss and optic nerve degeneration in GLAST-deficient mice, which leads to improved visual function as detected by mfERG (Figure 1).

IOP measurement in GLAST/ASK1 double-deficient mice. We have previously reported that GLAST-deficient mice show normal IOP compared with WT mice.[13] To determine the effect of ASK1 on IOP, we examined the IOP of ASK1$^{-/-}$, GLAST$^{+/-}$:ASK1$^{-/-}$ and GLAST$^{-/-}$:ASK1$^{-/-}$ mice. IOP measurements were carried out at around 2100 hours, when IOP is highest in mouse eyes.[19] The IOP values of ASK1$^{-/-}$, GLAST$^{+/-}$:ASK1$^{-/-}$ and GLAST$^{-/-}$:ASK1$^{-/-}$ mice were not significantly decreased compared with WT and GLAST$^{-/-}$ mice (Figure 5). These results suggest that the recovery of NTG-like pathology in GLAST$^{+/-}$:ASK1$^{-/-}$ and GLAST$^{-/-}$:ASK1$^{-/-}$ mice is IOP independent.

Role of oxidative stress and glutamate neurotoxicity in GLAST/ASK1 double-deficient mice. Oxidative stress has been proposed to contribute to RGC death in glaucoma, and a reduction in glutathione levels was reported in the plasma of human glaucoma patients.[15] Consistent with these findings, we have previously reported a decreased glutathione concentration in the retina of GLAST$^{-/-}$ mice.[13] To determine the effect of ASK1 on glutathione synthesis, we examined the glutathione concentration in the retina of 6 M ASK1$^{-/-}$ and GLAST$^{-/-}$:ASK1$^{-/-}$ mice and found that it was not significantly increased compared with WT and GLAST$^{-/-}$ mice, respectively (Figure 6a). In addition, the malondialdehyde concentration in the retina of ASK1$^{-/-}$ and GLAST$^{-/-}$:ASK1$^{-/-}$ mice was indistinguishable from that of WT and GLAST$^{-/-}$ mice, respectively (Figure 6b).

We have previously reported that intravitreal glutamate concentration is normal, but memantine, *N*-methyl-D-aspartate receptor antagonist, partially protected RGCs in GLAST$^{-/-}$ mice.[13] In addition, we showed that GLAST has a major role in glutamate uptake into Müller glial cells.[20] To explore the possibility that ASK1 is involved in glutamate transport, we examined glutamate uptake activity in Müller glial cells prepared from ASK1$^{-/-}$ and GLAST$^{+/-}$:ASK1$^{-/-}$ mice, and found that it was not significantly increased compared with WT and GLAST$^{+/-}$ mice, respectively (Figure 7). These findings suggest that ASK1 deficiency attenuates NTG-like degeneration without affecting the conditions of oxidative stress and glutamate neurotoxicity in GLAST-deficient mice.

Effect of ASK1-p38 mitogen-activated protein kinase (MAPK) signaling in Müller glial cells and RGCs. ASK1 is activated in response to cytotoxic stresses, including reactive oxygen species (ROS) and tumor necrosis factor (TNF), and relays these signals to p38 MAPK.[16,17] To determine whether this pathway is active in Müller glial cells, we first examined the effects of TNF on cultured Müller cells from WT and ASK1$^{-/-}$ mice. Western blot analysis demonstrated that stimulation of WT Müller cells with TNF leads to strong phosphorylation of p38 in a dose-dependent manner (Figure 8a). The activation of p38, however, was significantly suppressed in ASK1-deficient Müller cells (Figure 8a). Nitric oxide (NO) generated by inducible nitric oxide synthase (iNOS) is involved in retinal neuronal cell death,[21,22] and a previous study has reported that TNF-induced iNOS expression and NO release are suppressed by a specific inhibitor of p38 in mouse astrocytes.[23] These results suggest that the ASK1-p38 pathway regulates TNF-induced iNOS expression in Müller cells. To evaluate this possibility, we next examined iNOS

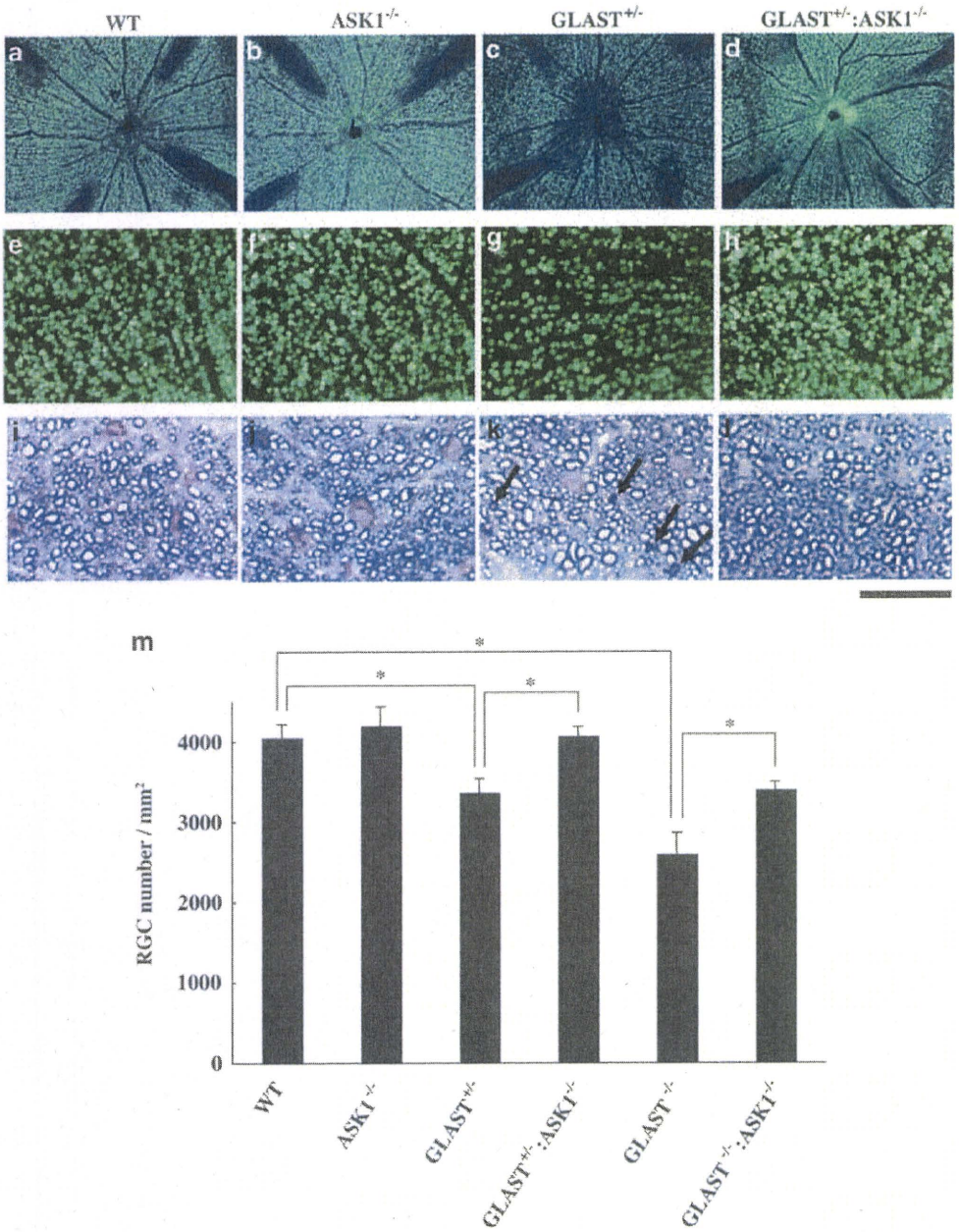

Figure 4 Effect of ASK1 on RGC and optic nerve degeneration. (**a–h**) Retrogradely labeled RGCs in WT, ASK1$^{-/-}$, GLAST$^{+/-}$ and GLAST$^{+/-}$:ASK1$^{-/-}$ mice. (**e–h**) Magnified images of (**a–d**), respectively. (**i–l**) Staining of semi-thin sections with toluidine blue revealed the presence of abnormally dark axonal profiles (arrowheads) and reduced axons in GLAST$^{+/-}$ mice (**k**), which was ameliorated in GLAST$^{+/-}$:ASK1$^{-/-}$ mice (**l**). (**m**) Quantification of labeled RGC number in WT, ASK1$^{-/-}$, GLAST$^{+/-}$, GLAST$^{+/-}$:ASK1$^{-/-}$, GLAST$^{-/-}$ and GLAST$^{-/-}$:ASK1$^{-/-}$ mice. Scale bar: 1 mm (**a–d**); 200 μm (**e–h**); 20 μm (**i–l**). *$P<0.05$

protein levels in cultured Müller cells. In untreated Müller cells, iNOS protein was almost absent, but TNF clearly increased iNOS expression levels (Figure 8b). Similar iNOS induction was detected in GLAST-deficient Müller cells (Figure 8b). However, TNF-induced iNOS expression was completely suppressed in ASK1-deficient Müller cells (Figure 8b). These results suggest that the ASK1-p38 pathway is required in Müller cells for the TNF-induced iNOS production, which may lead to the death of retinal neurons including RGCs. We further examined the direct effect of TNF on cultured RGCs.[18] TNF-induced cell death in cultured RGCs from ASK1-deficient mice was significantly decreased (41 ± 9%; $n=6$) compared with that from WT mice ($P<0.05$, Figure 8c). Taken together, loss of ASK1 prevents TNF-induced RGC death through both the direct pathway and the indirect pathway through Müller cells that is independent of GLAST.

Discussion

In this study, we show that ASK1 is associated with progressive RGC loss, glaucomatous optic nerve degeneration and visual disturbances in GLAST-deficient mice. We previously suggested the possibility that dysfunction of

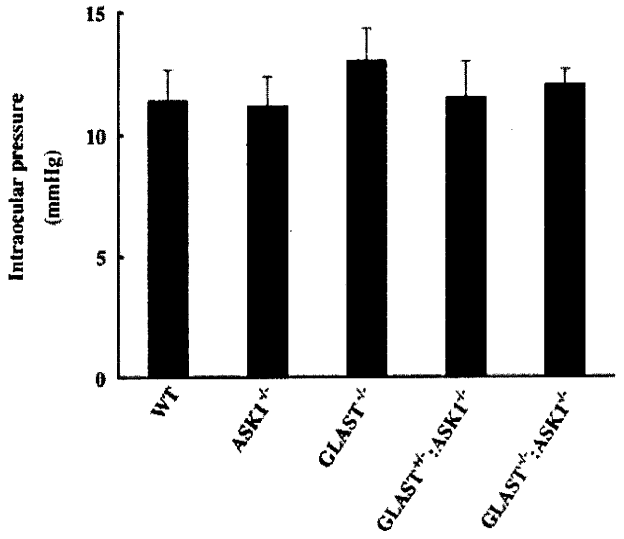

Figure 5 Effect of ASK1 on intraocular pressure in GLAST$^{+/-}$ and GLAST$^{-/-}$ mice. Intraocular pressure in GLAST$^{+/-}$:ASK1$^{-/-}$ and GLAST$^{-/-}$:ASK1$^{-/-}$ mice was not significantly decreased compared with GLAST$^{-/-}$ mice

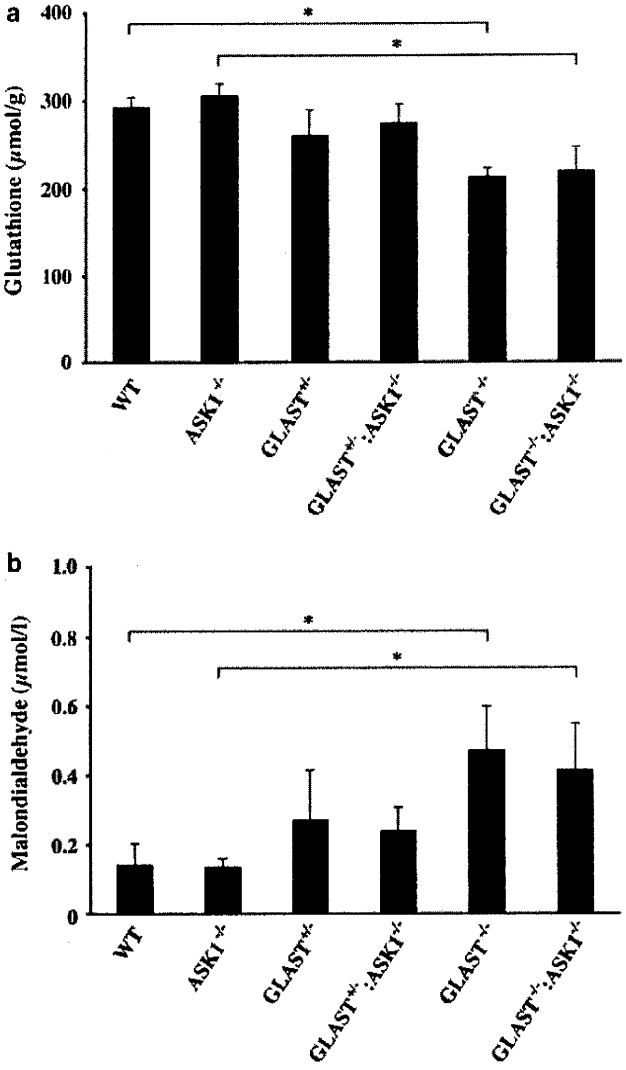

Figure 6 Effect of ASK1 on oxidative stress in GLAST$^{+/-}$ and GLAST$^{-/-}$ mice. (**a**) Mean glutathione concentration in whole retinas from WT, ASK1$^{-/-}$, GLAST$^{+/-}$, GLAST$^{+/-}$:ASK1$^{-/-}$, GLAST$^{-/-}$ and GLAST$^{-/-}$:ASK1$^{-/-}$ mice. (**b**) Malondialdehyde concentration in whole retinas from WT, ASK1$^{-/-}$, GLAST$^{+/-}$, GLAST$^{+/-}$:ASK1$^{-/-}$, GLAST$^{-/-}$ and GLAST$^{-/-}$:ASK1$^{-/-}$ mice. *$P<0.05$

GLAST (human EAAT1) has a role in RGC death in human NTG.[13] It has been reported that EAAT1 is downregulated in the retinas of human patients with glaucoma[14] and in fibroblasts from patients with Alzheimer's disease.[24] Considering the high frequency of glaucoma in Alzheimer's disease patients,[25] common mechanisms such as GLAST dysfunction might contribute to both diseases. Interestingly, ROS-mediated ASK1 activation is a key mechanism for amyloid beta (Aβ)-induced neurotoxicity, which has a central role in Alzheimer's disease.[26] The accumulation of Aβ is also observed in apoptotic RGCs in a rat model of glaucoma due to high IOP.[27] In this model, inhibiting amyloidogenic pathways by agents affecting multiple stages of the Aβ pathway reduces RGC apoptosis *in vivo*.[27] This suggests a new hypothesis for RGC death in glaucoma involving ASK1-dependent Aβ neurotoxicity, mimicking Alzheimer's disease.[28] In addition, multiple single-nucleotide polymorphisms in the Toll-like receptor 4 (*TLR4*) gene have been associated with the risk of NTG.[29] As ASK1 is required for innate immune responses dependent on TLR4,[30] TLR4-ASK1 signaling may be involved in the development of NTG. Taken together, these findings suggest that ASK1 may have roles in various neurodegenerative disorders, including glaucoma.[16–18]

Our present results demonstrate reduced RGC death, decreased axonal loss and mild visual disturbance in GLAST$^{+/-}$:ASK1$^{-/-}$ and GLAST$^{-/-}$:ASK1$^{-/-}$ mice, highlighting ASK1 as a potential therapeutic target for NTG. Loss of ASK1 had no effect on IOP (Figure 5), the production of malondialdehyde (Figure 6) or glutamate uptake activity by Müller cells (Figure 7). Whereas TNF-induced iNOS production was suppressed in ASK1-deficient Müller cells, and ASK1-deficient RGCs were more resistant to TNF-induced death compared with WT RGCs (Figure 8). Thus, in combination with conventional treatments to lower IOP, inhibition of ASK1 signaling may be useful in the treatment of glaucoma. In addition, we recently reported that interleukin-1 (IL-1) increases glutamate uptake by Müller cells, primarily through the activation of GLAST, and protects RGCs from glutamate neurotoxicity.[20,31] IL-1 is a mediator of brain injury induced by ischemia or trauma and has been implicated in chronic brain diseases, such as Alzheimer's disease, Parkinson's disease and multiple sclerosis.[32] Therefore, we need to examine the beneficial and detrimental roles of IL-1 during glaucoma *in vivo*. Furthermore, we are undertaking experiments to determine the neuroprotective effect of GLAST against neurotoxicity, axotomy and neuroinflammation in mice overexpressing GLAST.

A recent study has shown that upregulation of GLAST in Müller cells by glial cell line-derived neurotrophic factor (GDNF) and neurturin (NTN) is required to rescue RGCs following optic nerve transection.[33] As the receptors for GDNF and NTN are increased in Müller cells after RGC axotomy, the neuroprotective effects of GDNF and NTN may be indirect, at

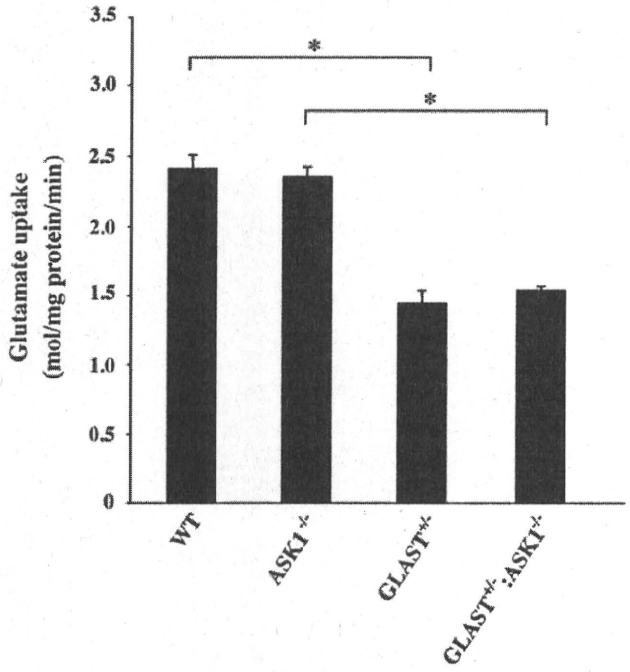

Figure 7 Glutamate uptake activity in Müller cells derived from WT, ASK1$^{-/-}$, GLAST$^{+/-}$ and GLAST$^{+/-}$:ASK1$^{-/-}$ mice. The data are presented as means ± S.E.M. of eight samples for each group. *$P<0.05$

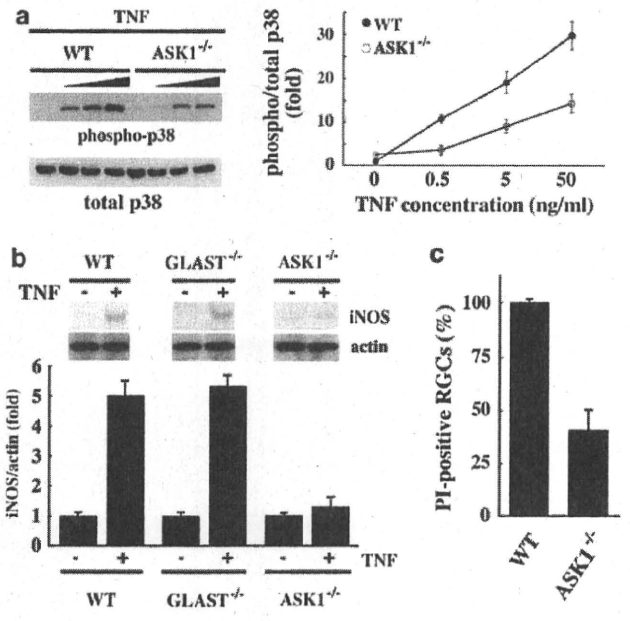

Figure 8 ASK1 is required for TNF-induced p38 activation and iNOS production in Müller glial cells. (**a**) Effect of ASK1 on TNF-induced p38 activation. Müller cells derived from WT or ASK1$^{-/-}$ mice were stimulated with the indicated concentration of TNF for 20 min, followed by immunoblot analysis of total and phosphorylated p38 in cell lysates. (**b**) Effect of GLAST and ASK1 on TNF-induced iNOS production. Müller cells derived from WT, GLAST$^{-/-}$ or ASK1$^{-/-}$ mice were stimulated for 16 h with TNF (50 ng/ml) or left unstimulated. (**c**) Effect of TNF on RGC death. RGCs derived from WT or ASK1$^{-/-}$ mice were treated for 2 days with TNF (400 ng/ml), and the number of PI-positive cells was counted. The data are presented as mean ± S.E.M. of six samples for each group

least partly, through the enhancement of glutamate uptake in Müller cells. Similar upregulation of the receptors for GDNF and NTN has been observed in a rat model of photoreceptor degeneration.[34,35] In this animal model, trophic factors such as nerve growth factor, brain-derived neurotrophic factor and basic fibroblast growth factor increase the production of multiple trophic factors in Müller cells, which indirectly leads to photoreceptor survival.[35–37] In addition, nerve growth factor eye drops may prevent the progress of human glaucoma.[38] In this study, we found that the loss of ASK1 prevented the activity of p38 and TNF-induced iNOS production in Müller cells (Figure 8). Recent studies have shown that TNF and NO can induce RGC death and participate in the pathophysiology of glaucoma.[39–41] Our results suggest that the ASK1-p38 pathway is involved in the process of TNF-induced RGC degeneration in neighboring glial cells, as well as in the RGC itself (Figure 8).[18] Taken together, these findings suggest that such a glial–neuronal network may be functional in various forms of neurodegenerative diseases and that ASK1, NO, GLAST and trophic factors in Müller cells have important roles in this network during glaucoma.[42,43] Thus, further efforts to discover new compounds that can enhance glutamate uptake and inhibit ASK1 signaling for a prolonged period may lead to the development of novel strategies for the management of glaucoma, including NTG.

Materials and Methods

Mice. Experiments were carried out using ASK1$^{-/-}$,[18] GLAST$^{+/-}$ and GLAST$^{-/-}$ mice[12,13] in accordance with the Tokyo Metropolitan Institute for Neuroscience *Guidelines for the Care and Use of Animals*. After mating ASK1$^{-/-}$ and GLAST$^{-/-}$ mice, GLAST$^{+/-}$:ASK1$^{+/-}$ mice were interbred to obtain GLAST$^{+/-}$:ASK1$^{-/-}$ and GLAST$^{-/-}$:ASK1$^{-/-}$ mice.

Histological and morphometric studies. Paraffin retinal sections of 7 μm thickness were cut through the optic nerve and stained with hematoxylin and eosin. RGC number and the extent of retinal degeneration were quantified in three ways.[18] First, the thickness of the IRL (between the internal limiting membrane and the interface of the outer plexiform layer and the outer nuclear layer) was analyzed. Second, in the same sections, the number of neurons in GCL was counted from one ora serrata through the optic nerve to the other ora serrata. Third, RGCs were retrogradely labeled from the superior colliculus with Fluoro-Gold (FG; Fluorochrome, Englewood, CO, USA). At 7 days after FG application, the eyes were enucleated, and the retinas were detached and prepared as flattened whole mounts in 4% PFA in 0.1 M PBS solution. The GCL was examined in whole-mounted retinas with fluorescence microscopy to determine RGC density. Four standard areas (0.04 mm^2) of each retina at a point 0.1 mm from the optic disc were randomly chosen. Labeled cells were counted by observers blinded to the identity of the mice, and the average number of RGCs/mm^2 was calculated. The changes in RGC number were expressed as a percentage of the WT control eyes.

For detailed morphological analysis, optic nerves were fixed in 2% glutaraldehyde and 2% paraformaldehyde in 0.1 M phosphate buffer overnight at 4°C. After dissection, the pieces of tissue were placed in 1% osmium tetroxide, and after dehydration, the pieces were embedded in Epon (Nisshin EM, Tokyo, Japan). Transverse semi-thin (1 μm) sections were stained with 0.2% toluidine blue in 1.0% sodium borate.[13,44]

IOP measurement. IOP was measured by a previously validated commercial rebound tonometer (TonoLab; Colonial Medical Supply, Franconia, NH, USA) in anesthetized mice as reported previously.[45] To minimize variation, the data were collected during a time window 4–6 min after injection of the anesthetic during which IOP plateaus. The animals were 6 months of age, and their body weights ranged from 22–36 g at the time of IOP measurement. As the 24-h IOP pattern in mouse eyes is biphasic, with IOP being highest around 2100 hours,[19] we examined IOP between 2000 and 2300 hours.

mfERG. Mice (3 months old) were anesthetized by intraperitoneal injection of a mixture of xylazine (10 mg/kg) and ketamine (25 mg/kg). The pupils were dilated with 0.5% phenylephrine hydrochloride and 0.5% tropicamide. mfERGs were recorded using a VERIS 6.0 system (Electro-Diagnostic Imaging, Redwood City, CA, USA). The visual stimulus consisted of seven hexagonal areas scaled with eccentricity. The stimulus array was displayed on a high-resolution black and white monitor driven at a frame rate of 100 Hz. The second-order kernel, which is impaired in patients with glaucoma, was analyzed.[13,44]

Malondialdehyde and glutathione assay. The concentrations of malondialdehyde and glutathione were measured using the Bioxytech LPO-586 (Oxis Research, Beverly Hills, CA, USA) and Glutathione Assay Kit (Cayman Chemical, Ann Arbor, MI, USA), according to the manufacturers' protocols.

Glutamate uptake assay. Glutamate uptake assay in primary cultured Müller cells was carried out as previously reported.[20,31] Müller cells were cultured in 5.5 mM glucose-containing DMEM supplemented with 10% fetal bovine serum. The culture media were replaced with a modified Hanks' balanced salt solution (HBSS) for a 20-min preincubation, before the addition of 0.025 mCi/ml L-[^{3}H]-glutamate (Amersham, Uppsala, Sweden) and 100 μM unlabeled glutamate to the media. Uptake was terminated after 7 min by three washes in ice-cold HBSS, immediately followed by cell lysis in 0.1 M NaOH. Aliquots were taken for scintillation counting, and protein concentration was determined using BSA standards.

Immunoblot analysis. Primary Müller cells were obtained as previously reported[35–37] and treated with TNF at various concentrations for 20 min or 16 h. Immunoblotting was carried out as previously reported.[20,31] Membranes were incubated with antibodies against p38 (1 : 1000; BD Biosciences Pharmingen, San Diego, CA, USA), phospho-p38 (1 : 1000; BD Biosciences Pharmingen) or iNOS (1 : 1000; BD Biosciences Pharmingen).

Assessment of TNF-induced cell death in cultured RGCs. RGCs derived form WT and ASK1$^{-/-}$ mice were seeded at a density of 5×10^4 cells per well and cultured with 0.1 ml of medium on a 96-well culture plate.[18] After 2 days, they were stimulated with 400 ng/ml of TNF for 2 days, and dying RGC number was counted after staining with propidium iodide.

Statistics. For statistical comparison of two samples, we used a two-tailed Student's *t*-test. Data are presented as the mean ± S.E.M. $P<0.05$ was regarded as statistically significant.

Conflict of interest

The authors declare no conflict of interest.

Acknowledgements. We thank Atsuko Kimura and Rikako Shimizu for technical assistance. This work was supported by the Ministry of Education, Culture, Sports, Science and Technology of Japan (KN, KT, HI, TH); the Ministry of Health, Labour and Welfare of Japan (YM, KT, TH); the Japan Society for the Promotion of Science for Young Scientists (CH); the Welfare and Health Funds from the Tokyo Metropolitan Government (YM); the Uehara Memorial Foundation; the Naito Foundation; the Suzuken Memorial Foundation; the Daiwa Securities Health Foundation; the Takeda Science Foundation and the Japan Medical Association (TH).

1. Quigley HA. Number of people with glaucoma worldwide. *Br J Ophthalmol* 1996; **80**: 389–393.
2. Wiggs JL. Genetic etiologies of glaucoma. *Arch Ophthalmol* 2007; **125**: 30–37.
3. Seki M, Lipton SA. Targeting excitotoxic/free radical signaling pathways for therapeutic intervention in glaucoma. *Prog Brain Res* 2008; **173**: 495–510.
4. Lindsey JD, Weinreb RN. Elevated intraocular pressure and transgenic applications in the mouse. *J Glaucoma* 2005; **14**: 318–320.
5. John SW, Smith RS, Savinova OV, Hawes N, Chang B, Turnbull D *et al.* Essential iris atrophy, pigment dispersion, and glaucoma in DBA/2J mice. *Invest Ophthalmol Vis Sci* 1998; **39**: 951–962.
6. Chiu K, Chang R, So KF. Laser-induced chronic ocular hypertension model on SD rats. *J Vis Exp* 2007; **10**: 549.
7. Iwase A, Suzuki Y, Araie M, Yamamoto T, Abe H, Shirato S *et al.* The prevalence of primary open-angle glaucoma in Japanese: the Tajimi Study. *Ophthalmology* 2004; **111**: 1641–1648.
8. Zhang X, Cheng M, Chintala SK. Optic nerve ligation leads to astrocyte-associated matrix metalloproteinase-9 induction in the mouse retina. *Neurosci Lett* 2004; **356**: 140–144.
9. Tanaka K, Watase K, Manabe T, Yamada K, Watanabe M, Takahashi K *et al.* Epilepsy and exacerbation of brain injury in mice lacking the glutamate transporter GLT-1. *Science* 1997; **276**: 1699–1702.
10. Watase K, Hashimoto K, Kano M, Yamada K, Watanabe M, Inoue Y *et al.* Motor discoordination and increased susceptibility to cerebellar injury in GLAST mutant mice. *Eur J Neurosci* 1998; **10**: 976–988.
11. Matsugami TR, Tanemura K, Mieda M, Nakatomi R, Yamada K, Kondo T *et al.* Indispensability of the glutamate transporters GLAST and GLT1 to brain development. *Proc Natl Acad Sci USA* 2006; **103**: 12161–12166.
12. Harada T, Harada C, Watanabe M, Inoue Y, Sakagawa T, Nakayama N *et al.* Functions of the two glutamate transporters GLAST and GLT-1 in the retina. *Proc Natl Acad Sci USA* 1998; **95**: 4663–4666.
13. Harada T, Harada C, Nakamura K, Quah HA, Okumura A, Namekata K *et al.* The potential role of glutamate transporters in the pathogenesis of normal tension glaucoma. *J Clin Invest* 2007; **117**: 1763–1770.
14. Naskar R, Vorwerk CK, Dreyer EB. Concurrent downregulation of a glutamate transporter and receptor in glaucoma. *Invest Ophthalmol Vis Sci* 2000; **41**: 1940–1944.
15. Gherghel D, Griffiths HR, Hilton EJ, Cunliffe IA, Hosking SL. Systemic reduction in glutathione levels occurs in patients with primary open-angle glaucoma. *Invest Ophthalmol Vis Sci* 2005; **46**: 877–883.
16. Nishitoh H, Kadowaki H, Nagai A, Maruyama T, Yokota T, Fukutomi H *et al.* ALS-linked mutant SOD1 induces ER stress- and ASK1-dependent motor neuron death by targeting Derlin-1. *Genes Dev* 2008; **22**: 1451–1464.
17. Hattori K, Naguro I, Runchel C, Ichijo H. The roles of ASK family proteins in stress responses and diseases. *Cell Commun Signal* 2009; **24**: 7–9.
18. Harada C, Nakamura K, Namekata K, Okumura A, Mitamura Y, Iizuka Y *et al.* Role of apoptosis signal-regulating kinase 1 in stress-induced neural cell apoptosis *in vivo*. *Am J Pathol* 2006; **168**: 261–269.
19. Aihara M, Lindsey JD, Weinreb RN. Twenty-four-hour pattern of mouse intraocular pressure. *Exp Eye Res* 2003; **77**: 681–686.
20. Namekata K, Harada C, Guo X, Kikushima K, Kimura A, Fuse N *et al.* Interleukin-1 attenuates normal tension glaucoma-like retinal degeneration in EAAC1 deficient mice. *Neurosci Lett* 2009; **465**: 160–164.
21. Hangai M, Yoshimura N, Hiroi K, Mandai M, Honda Y. Inducible nitric oxide synthase in retinal ischemia-reperfusion injury. *Exp Eye Res* 1996; **63**: 501–509.
22. Goureau O, Régnier-Ricard F, Courtois Y. Requirement for nitric oxide in retinal neuronal cell death induced by activated Müller glial cells. *J Neurochem* 1999; **72**: 2506–2515.
23. Da Silva J, Pierrat B, Mary JL, Lesslauer W. Blockade of p38 mitogen-activated protein kinase pathway inhibits inducible nitric-oxide synthase expression in mouse astrocytes. *J Biol Chem* 1997; **272**: 28373–28380.
24. Zoia CP, Tagliabue E, Isella V, Begni B, Fumagalli L, Brighina L *et al.* Fibroblast glutamate transport in aging and in AD: correlations with disease severity. *Neurobiol Aging* 2005; **26**: 825–832.
25. Tamura H, Kawakami H, Kanamoto T, Kato T, Yokoyama T, Sasaki K *et al.* High frequency of open-angle glaucoma in Japanese patients with Alzheimer's disease. *J Neurol Sci* 2006; **246**: 79–83.
26. Kadowaki H, Nishitoh H, Urano F, Sadamitsu C, Matsuzawa A, Takeda K *et al.* Amyloid beta induces neuronal cell death through ROS-mediated ASK1 activation. *Cell Death Differ* 2005; **12**: 19–24.
27. Guo L, Salt TE, Luong V, Wood N, Cheung W, Maass A *et al.* Targeting amyloid-beta in glaucoma treatment. *Proc Natl Acad Sci USA* 2007; **104**: 13444–13449.
28. McKinnon SJ. Glaucoma: ocular Alzheimer's disease? *Front Biosci* 2003; **8**: 1140–1156.
29. Shibuya E, Meguro A, Ota M, Kashiwagi K, Mabuchi F, Iijima H *et al.* Association of Toll-like receptor 4 gene polymorphisms with normal tension glaucoma. *Invest Ophthalmol Vis Sci* 2008; **49**: 4453–4457.
30. Matsuzawa A, Saegusa K, Noguchi T, Sadamitsu C, Nishitoh H, Nagai S *et al.* ROS-dependent activation of the TRAF6-ASK1-p38 pathway is selectively required for TLR4-mediated innate immunity. *Nat Immunol* 2005; **6**: 587–592.
31. Namekata K, Harada C, Kohyama K, Matsumoto Y, Harada T. Interleukin-1 stimulates glutamate uptake in glial cells by accelerating membrane trafficking of Na^+/K^+-ATPase via actin depolymerization. *Mol Cell Biol* 2008; **28**: 3273–3280.
32. Rothwell NJ, Luheshi GN. Interleukin 1 in the brain: biology, pathology and therapeutic target. *Trends Neurosci* 2000; **23**: 618–625.
33. Koeberle PD, Bähr M. The upregulation of GLAST-1 is an indirect antiapoptotic mechanism of GDNF and neurturin in the adult CNS. *Cell Death Differ* 2008; **15**: 471–483.
34. Jomary C, Thomas M, Grist J, Milbrandt J, Neal MJ, Jones SE. Expression patterns of neurturin and its receptor components in developing and degenerative mouse retina. *Invest Ophthalmol Vis Sci* 1999; **40**: 568–574.
35. Harada C, Harada T, Quah HM, Maekawa F, Yoshida K, Ohno S *et al.* Potential role of glial cell line-derived neurotrophic factor receptors in Müller glial cells during light-induced retinal degeneration. *Neuroscience* 2003; **122**: 229–235.

36. Harada T, Harada C, Kohsaka S, Wada E, Yoshida K, Ohno S *et al.* Microglia-Müller glia cell interactions control neurotrophic factor production during light-induced retinal degeneration. *J Neurosci* 2002; **22**: 9228–9236.
37. Harada T, Harada C, Nakayama N, Okuyama S, Yoshida K, Kohsaka S *et al.* Modification of glial-neuronal cell interactions prevents photoreceptor apoptosis during light-induced retinal degeneration. *Neuron* 2000; **26**: 533–541.
38. Lambiase A, Aloe L, Centofanti M, Parisi V, Mantelli F, Colafrancesco V *et al.* Experimental and clinical evidence of neuroprotection by nerve growth factor eye drops: implications for glaucoma. *Proc Natl Acad Sci USA* 2009; **106**: 13469–13474.
39. Osborne NN. Pathogenesis of ganglion 'cell death' in glaucoma and neuroprotection: focus on ganglion cell axonal mitochondria. *Prog Brain Res* 2008; **173**: 339–352.
40. Nakazawa T, Nakazawa C, Matsubara A, Noda K, Hisatomi T, She H *et al.* Tumor necrosis factor-alpha mediates oligodendrocyte death and delayed retinal ganglion cell loss in a mouse model of glaucoma. *J Neurosci* 2006; **26**: 12633–12641.
41. Toda N, Nakanishi-Toda M. Nitric oxide: ocular blood flow, glaucoma, and diabetic retinopathy. *Prog Retin Eye Res* 2007; **26**: 205–238.
42. Bringmann A, Iandiev I, Pannicke T, Wurm A, Hollborn M, Wiedemann P *et al.* Cellular signaling and factors involved in Müller cell gliosis: neuroprotective and detrimental effects. *Prog Retin Eye Res* 2009; **28**: 423–451.
43. Harada C, Mitamura Y, Harada T. The role of cytokines and trophic factors in epiretinal membranes: involvement of signal transduction in glial cells. *Prog Retin Eye Res* 2006; **25**: 149–164.
44. Guo X, Harada C, Namekata K, Kikushima K, Mitamura Y, Yoshida H *et al.* Effect of geranylgeranylacetone on optic neuritis in experimental autoimmune encephalomyelitis. *Neurosci Lett* 2009; **462**: 281–285.
45. Haddadin RI, Oh DJ, Kang MH, Filippopoulos T, Gupta M, Hart L *et al.* SPARC-null mice exhibit lower intraocular pressures. *Invest Ophthalmol Vis Sci* 2009; **50**: 3771–3777.

Dock3 induces axonal outgrowth by stimulating membrane recruitment of the WAVE complex

Kazuhiko Namekata[a], Chikako Harada[a,b], Choji Taya[c], Xiaoli Guo[a], Hideo Kimura[d], Luis F. Parada[b], and Takayuki Harada[a,b,1]

[a]Department of Molecular Neurobiology, Tokyo Metropolitan Institute for Neuroscience, Fuchu, Tokyo 183-8526, Japan; [b]Department of Developmental Biology and Kent Waldrep Foundation Center for Basic Research on Nerve Growth and Regeneration, University of Texas Southwestern Medical Center, Dallas, TX 75390; [c]Department of Laboratory Animal Science, Tokyo Metropolitan Institute of Medical Science, Setagaya, Tokyo 156-8506, Japan; and [d]Department of Molecular Genetics, National Institute of Neuroscience, National Center of Neurology and Psychiatry, Kodaira, Tokyo 187-8502, Japan

Edited by Thomas C. Südhof, Stanford University School of Medicine, Palo Alto, CA, and approved March 16, 2010 (received for review December 18, 2009)

Atypical Rho-guanine nucleotide exchange factors (Rho-GEFs) that contain Dock homology regions (DHR-1 and DHR-2) are expressed in a variety of tissues; however, their functions and mechanisms of action remain unclear. We identify key conserved amino acids in the DHR-2 domain that are critical for the catalytic activity of Dock-GEFs (Dock1–4). We further demonstrate that Dock-GEFs directly associate with WASP family verprolin-homologous (WAVE) proteins through the DHR-1 domain. Brain-derived neurotrophic factor (BDNF)-TrkB signaling recruits the Dock3/WAVE1 complex to the plasma membrane, whereupon Dock3 activates Rac and dissociates from the WAVE complex in a phosphorylation-dependent manner. BDNF induces axonal sprouting through Dock-dependent Rac activation, and adult transgenic mice overexpressing Dock3 exhibit enhanced optic nerve regeneration after injury without affecting WAVE expression levels. Our results highlight a unique mechanism through which Dock-GEFs achieve spatial and temporal restriction of WAVE signaling, and identify Dock-GEF activity as a potential therapeutic target for axonal regeneration.

Dock family proteins | brain-derived neurotrophic factor | Fyn | axonal regeneration | optic nerve

The Rho-family GTPases (Rho-GTPases, including Rac1, Cdc42, and RhoA), which are best known for their roles in regulating the actin cytoskeleton, have been implicated in a broad spectrum of biological functions, such as cell motility and invasion, cell growth, cell survival, cell polarity, clearance of apoptotic cells, membrane protrusion, and axonal guidance (1, 2). Activation signals from Rac1 and Cdc42 are relayed to the actin-nucleating complex Arp2/3 by a family of proteins that includes Wiskott–Aldrich syndrome protein (WASP) and WASP family verprolin-homologous protein (WAVE) (3, 4). Rho-GTPase activation is mediated by guanine nucleotide exchange factors (GEFs), which share common motifs: the Dbl-homology (DH) domain, which mediates nucleotide exchange (5), and the pleckstrin homology (PH) domain, which targets proteins to membranes and mediates protein–protein interactions (6). Dock1 (Dock180)–related proteins are a new family of Rho-GEFs that lack the DH/PH domains. Instead, Dock family proteins are characterized by two evolutionarily conserved protein domains, termed Dock homology regions 1 and 2 (DHR-1 and DHR-2, respectively) (7). However, the precise functions of the DHR domains are poorly understood. In mammals, there are 11 Dock1-related proteins (Dock1–11). We previously reported that one of the new Rho-GEFs, Dock3, also known as MOCA (modifier of cell adhesion protein), is specifically expressed in the central nervous system (CNS) and induces membrane spreading by activating Rac1 (8).

Neurotrophins are a small family of evolutionarily well-conserved neuropeptides that function in neural cell survival, development, and vertebrate CNS function (9, 10). Neurotrophins, such as brain-derived neurotrophic factor (BDNF), bind to two classes of receptors, the Trk receptor tyrosine kinase family (TrkA, TrkB, TrkC) and the low-affinity receptor p75 ($p75^{NTR}$), leading to complex functional interactions (11, 12). Recent studies have demonstrated that neurotrophins play important roles during gastrulation, in the differentiation of hepatic stellate cells, and in neurulation, through the regulation of Rho-GTPases (9, 13, 14). Considering their relatively ubiquitous expression patterns, it is conceivable that Dock family members, in combination with neurotrophins, could be involved in the development and function of a variety of organs (15–17).

Here, we report that the atypical Rho-GEFs Dock1–4 share key amino acids within the DHR-2 domain that are critical for catalytic activity, and furthermore, that they bind directly to WAVE proteins through the DHR-1 domain. Moreover, we provide both in vitro and in vivo evidence that neuron-specific Dock3 plays a critical role in the membrane trafficking of WAVE proteins and also participates in axonal outgrowth in the adult CNS as an essential downstream component of BDNF-TrkB signaling.

Results

Identification of Critical Residues Involved in GEF Catalytic Activity. To identify residues critical for Rac1 activation, we constructed several Dock3 DHR-2 domain deletion mutants (Fig. 1*A*) and measured their catalytic activity with a GST-CRIB assay (Fig. 1*B*). All of the deletion mutants failed to activate Rac1 (Fig. 1*B*), indicating that amino acids 1358–1375 are required for Dock3-mediated GEF activity. We next introduced single alanine mutations into each of the 18 DHR-2 domain amino acids within full-length Dock3 and found that mutation at F1359, Y1360, G1361, Y1373, or V1374 completely abolished Rac1 activation (Fig. 1*C*) without affecting its ability to interact with Rac1 (Fig. 1*D*). Because the DHR-2 domain is highly conserved among Dock1–4 (Fig. 1*A*), the five single alanine substitutions corresponding to those found in Dock3 were introduced into Dock1, Dock2, and Dock4. All of the mutations drastically reduced Rac1 activation (Fig. S1), demonstrating that these five amino acids of the DHR-2 domain are critical for GEF catalytic activity in all Rac-specific Dock family members.

Dock3 Regulates Axonal Outgrowth. To evaluate whether Dock3 induces axonal outgrowth, we transfected primary cultured hippocampal neurons with plasmid encoding Dock3. Overexpression of Dock3 significantly stimulated axonal outgrowth compared with the control (Fig. 2*A* and *B*). As neurotrophic factors such as BDNF may also regulate Rac1 activation (18), we next examined whether Dock3 and BDNF have a synergistic effect on axonal outgrowth. Overexpression of wild-type (WT) Dock3 increased BDNF-mediated

Author contributions: K.N. and T.H. designed research; K.N., C.H., C.T., and X.G. performed research; K.N., C.T., H.K., and L.F.P. contributed new reagents/analytic tools; K.N., C.H., X.G., L.F.P., and T.H. analyzed data; and K.N., L.F.P., and T.H. wrote the paper.

The authors declare no conflict of interest.

This article is a PNAS Direct Submission.

[1]To whom correspondence should be addressed. E-mail: harada-tk@igakuken.or.jp.

This article contains supporting information online at www.pnas.org/cgi/content/full/0914514107/DCSupplemental.

www.pnas.org/cgi/doi/10.1073/pnas.0914514107

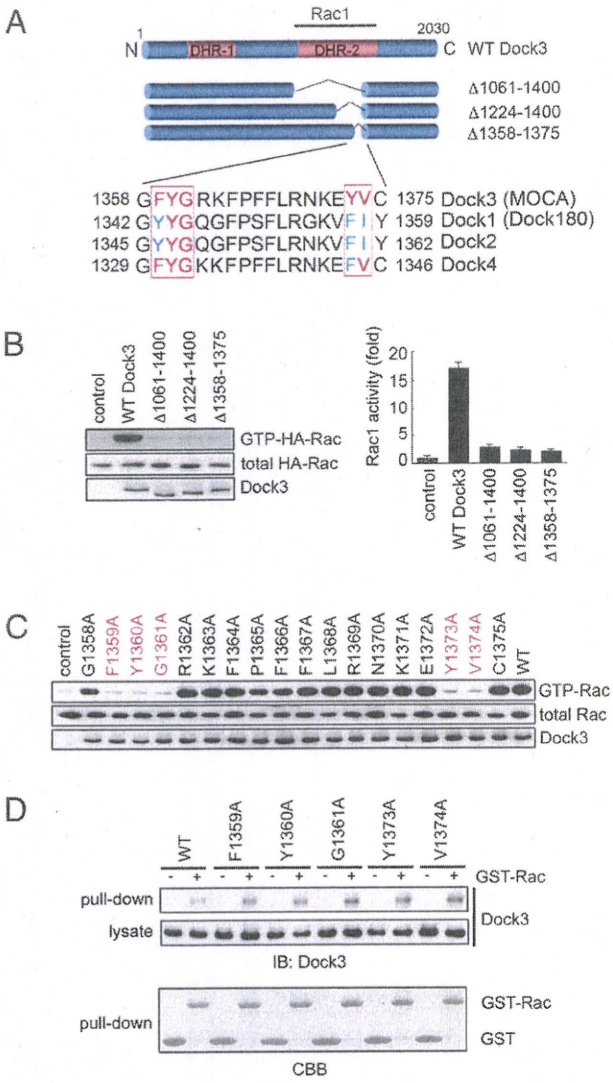

Fig. 1. Identification of residues critical for the catalytic activity of Dock family members. (*A*) Domain organization and sequence alignments of Dock1–4. (*B*) (*Left*) Cos-7 cells were transfected with Dock3 deletion mutants. Lysates were subjected to a GST-CRIB assay. (*Right*) Quantitation of GTP-Rac. (*C*) Cos-7 cells were transfected with the indicated alanine-substitution mutants of Dock3. Lysates were subjected to a GST-CRIB assay. (*D*) Cos-7 cells were transfected with the indicated alanine-substitution mutants of Dock3. Lysates were incubated with GST-Rac and glutathione-Sepharose. Bound proteins were subjected to immunoblot analysis with anti-Dock3 antibody. (*Lower*) Coomassie Brilliant Blue (CBB) staining of GST-fusion proteins used in this experiment.

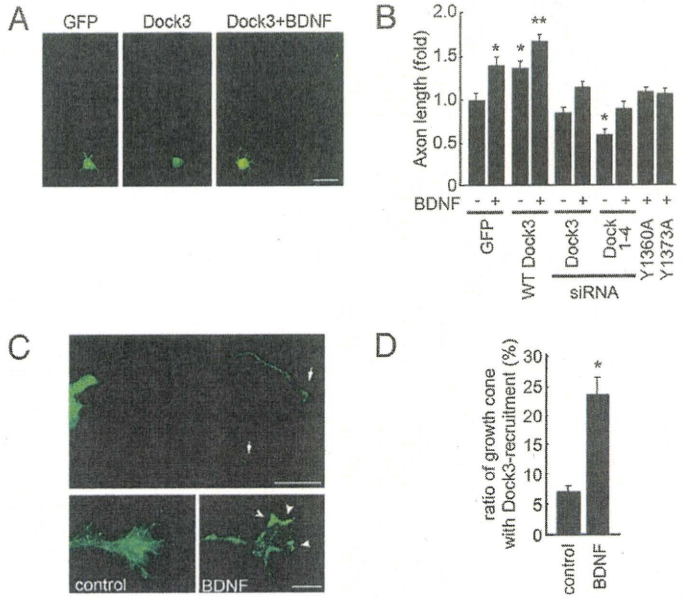

Fig. 2. Dock3 enhances BDNF-mediated axonal growth. (*A*) Hippocampal neurons were transfected with Dock3 and cultured in the presence or absence of BDNF for 3 days. (Scale bar, 20 μm.) (*B*) Hippocampal neurons transfected and treated as shown at the *x* axis were fixed at 3 days in vitro, and axon length was measured. $n = 30$ per experimental condition. Data are mean ± SEM of three independent experiments. $^*P < 0.05$, $^{**}P < 0.01$. (*C*) Expression of Dock3 in retinal explant cultures. (*Upper*) Dock3 expression in growth cones (arrows). (*Lower*) High magnification of growth cones. Arrowheads indicate Dock3 recruitment to plasma membrane after BDNF treatment. (Scale bars, 50 μm in upper and 10 μm in lower.) (*D*) Ratio of growth cones in which Dock3 was recruited to plasma membrane. Data are mean ± SEM; $n = 20$ for each experimental condition. $^*P < 0.01$.

axonal outgrowth (Fig. 2 *A* and *B*), whereas Dock3 siRNA for downregulating endogenous Dock3 inhibited the effect of BDNF (Fig. 2*B*). Combinatorial siRNA to Dock1–4 decreased the baseline axon length (Fig. 2*B*). In addition, Dock3^{Y1360A} and Dock3^{Y1373A} also inhibited the effect of BDNF (Fig. 2*B*). BDNF-mediated axonal outgrowth and Rac1 activation were observed in cultured neurons from WT and p75^{NTR} KO mice, but not from TrkB KO mice (Fig. S2). Trk receptor-specific inhibitor K252a and overexpression of dominant-negative Rac1 (Rac1 N17) suppressed BDNF-mediated axonal outgrowth (Fig. S2). Furthermore, we found that Dock3 is expressed in retinal ganglion cells (RGCs) and has a synergistic effect with BDNF on axonal outgrowth in cultured RGCs (Fig. S3). In retinal explant cultures, Dock3 protein was concentrated in growth cones (arrows in Fig. 2*C*) and was diffuse in cytoplasm (control panel in Fig. 2*C*). However, BDNF treatment rearranged Dock3 staining to the cell periphery (arrowheads in Fig. 2 *C* and *D*). These data demonstrate that Dock3 act in concert, upstream of Rac1, to promote axonal outgrowth through TrkB receptor signaling.

Interaction of Dock3 and Fyn at the Growth Cone. One consequence of the presence of BDNF in neurons is the activation of Fyn and its association with the TrkB receptor (19). Indeed, BDNF induced Fyn activation via phosphorylation at Y416 in primary cultured hipocampal neurons (Fig. 3*A*). Because the proline-rich motif of Dock3 binds to SH3 domain-containing proteins (8), we next examined whether Fyn, which also possesses an SH3 domain, interacts with Dock3. A GST-fusion protein of the proline-rich Dock3 C terminus (amino acids 1773–2028) coprecipitated Fyn in lysates of mouse brain as well as Fyn-transfected Cos-7 cells (Fig. 3*B*). In addition, a His-tag pull-down assay in Cos-7 cells transfected with His-tagged Dock3 together with WT Fyn, constitutively active Fyn^{Y528F}, or ΔSH3 Fyn^{Y528F} (20), confirmed the SH3 domain requirement and preferential binding to the active form of Fyn (Fig. 3*C*). In contrast, Fyn failed to bind to Elmo (21), which interacts with Dock1–4 and enhances their GEF activities (Fig. S4). Thus, the BDNF/TrkB-dependent activation and association with Fyn is specific. Consistent with the activated TrkB association with Fyn and interaction with Dock3, Dock3 translocated from cytosol to the membrane in SY5Y cells transfected with TrkB and Fyn^{Y528F} in the presence of BDNF, but not in cells transfected with TrkB and ΔSH3 Fyn^{Y528F} (Fig. 3*D*). In addition, BDNF-treated retinal explants exhibit colocalization of Dock3 and Fyn at the peripheral regions of the growth cone (arrowheads in Fig. 3*E*). These results are consistent with a model whereby BDNF-TrkB signaling induces the formation of a protein complex of Dock3 at the plasma membrane (Fig. 2 *C* and *D*). We further constructed a mutant Dock3 lacking Fyn binding domain (Δ1773–

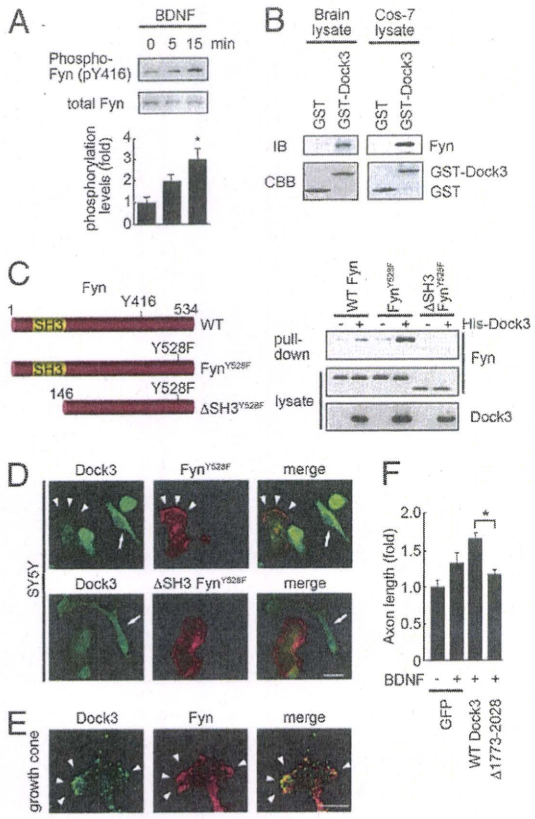

Fig. 3. BDNF induces direct binding of Dock3 and Fyn in the growth cone. (*A*) Hippocampal neurons were transfected with WT Fyn and stimulated with BDNF for the indicated times. Lysates were subjected to immunoblot analysis with anti-Fyn^{pY416} or total Fyn antibodies. (*Lower*) expression levels of phosphorylated Fyn. Data are mean ± SEM of three independent experiments. $*P < 0.05$. (*B*) Lysates from mouse brain and Cos-7 cells transfected with WT Fyn were incubated with a GST-fusion protein of the Dock3 proline-rich domain. Bound proteins were subjected to immunoblot (IB) analysis with an anti-Fyn antibody. (*Lower*) Coomassie Brilliant Blue (CBB) staining of the GST-fusion proteins used in this experiment. (*C*) (*Left*) Schematic diagram of the WT and mutant Fyn constructs used in this assay. (*Right*) Lysates from Cos-7 cells transfected as shown at the top of the images were subjected to a His-tag pull-down assay with antibodies against Fyn and Dock3. (*D*) SY5Y cells were transfected with TrkB and Fyn^{Y528F} or ΔSH3 Fyn^{Y528F} and treated with BDNF. Arrowheads indicate colocalization of Dock3 (green) and WAVE1 (red) at the peripheral region. Arrow indicates a nontransfected cell. (Scale bar, 20 μm.) (*E*) Colocalization of endogenous Dock3 (green) and Fyn (red) in growth cone of retinal explant cultures after BDNF treatment. (Scale bar, 10 μm.) (*F*) Hippocampal neurons transfected and treated as shown at the *x* axis were fixed at 3 days in vitro and axon length measured. $n = 30$ for each experimental condition. Data are mean ± SEM of three independent experiments. $*P < 0.05$.

2028) and found that this mutant failed to stimulate BDNF-induced axonal outgrowth (Fig. 3*F*).

Direct Interaction of Dock3 and WAVE Proteins. Because WAVE proteins play a major role in Rac-induced actin dynamics, including actin nucleation and polymerization (3, 4), we speculated that they could be involved in Dock3-mediated axonal outgrowth. To investigate the possibility that WAVE1 can directly bind to Dock3, we performed a His-tag pull-down assay using WT Dock3 or several Dock3 truncation mutants. We found that Dock3 directly bound to WAVE1 at the DHR-1 domain (Fig. 4*A*). We next constructed a mutant that lacks the DHR-1 domain (ΔDHR-1) and determined that this mutant also failed to bind to WAVE1 (Fig. 4*B*). We further confirmed that the DHR-1 domain of Dock3 was required to mediate WAVE1–3 binding (Fig. 4*C*). Indeed, this interaction between Dock and WAVE proteins can be generalized (Fig. S5). In addition, we

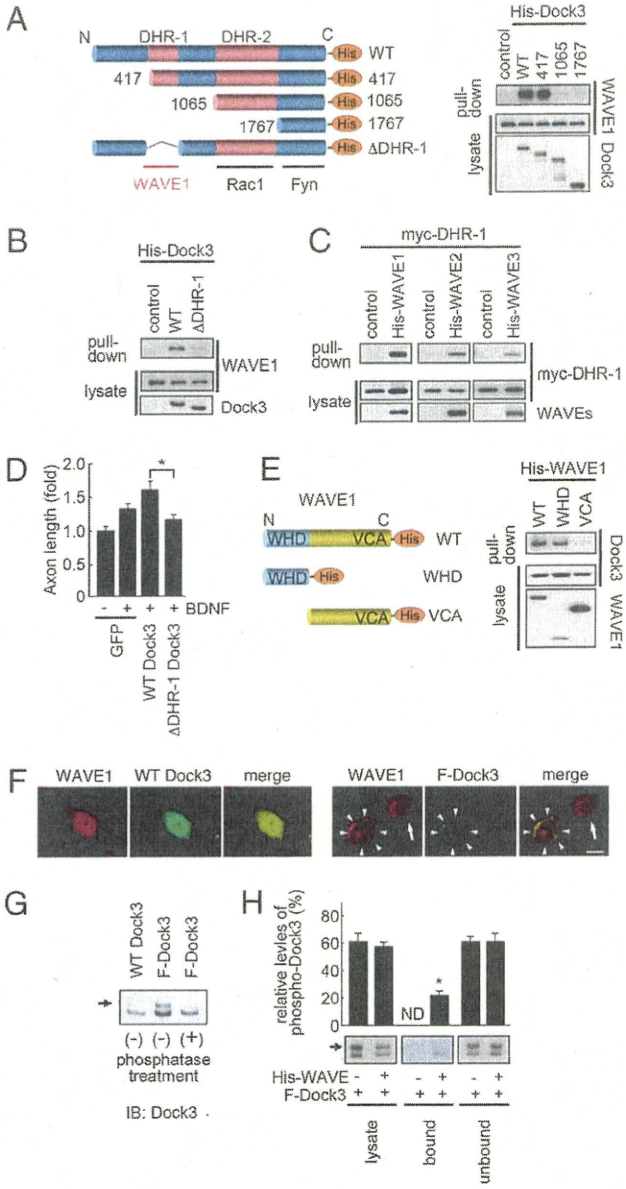

Fig. 4. Phosphorylation of Dock3 regulates its interaction with WAVE. (*A*) (*Left*) schematic diagram of the WT and mutant Dock3 constructs used in this assay. (*Right*) Lysates from Cos-7 cells transfected as shown at the top of the images were subjected to a His-tag pull-down assay with antibodies against WAVE1 and Dock3. (*B*) Lysates from Cos-7 cells transfected as shown at the top of the images were subjected to a His-tag pull-down assay with antibodies against WAVE1 and Dock3. (*C*) Lysates from Cos-7 cells transfected as shown at the top of the images were subjected to a His-tag pull-down assay with antibodies against myc-tag, WAVE1, WAVE2, and WAVE3. (*D*) Hippocampal neurons transfected and treated as shown at the *x* axis were fixed at 3 days in vitro, and axon length was measured. $n = 30$ for each experimental condition. Data are mean ± SEM of three independent experiments. $*P < 0.05$. (*E*) (*Left*) Schematic diagram of the WT and mutant WAVE1 constructs used in this assay. (*Right*) Lysates from Cos-7 cells transfected as shown at the top of the images were subjected to a His-tag pull-down assay with antibodies against Dock3 and WAVE1. (*F*) SY5Y cells transfected with WT Dock3 or F-Dock3 were probed with antibodies against WAVE1 (red) and Dock3 (green). Arrowheads indicate WAVE1 protein at the peripheral region. The arrow indicates a nontransfected cell. (Scale bar, 10 μm.) (*G*) Lysates from Cos-7 cells transfected with WT Dock3 or F-Dock3 were subjected to immunoblot analysis with an anti-Dock3 antibody. Arrow indicates phosphorylated Dock3. (*H*) (*Upper*) Relative expression levels of phosphorylated Dock3 to total Dock3. (*Lower*) Lysates from Cos-7 cells transfected as shown at the bottom of the images were subjected to a His-tag pull-down assay. Bound and unbound proteins were subjected to immunoblot analysis with an anti-Dock3 antibody. Arrow indicates phosphorylated Dock3.

demonstrated that ΔDHR-1 failed to stimulate BDNF-induced axonal outgrowth in hippocampal neurons (Fig. 4*D*). We next prepared both WT and two mutant forms of WAVE1 constructs and found that one mutant that lacks the WAVE-homology domain (WHD) failed to bind to WT Dock3 (Fig. 4*E*). Based on the preceding data, we hypothesized that membrane targeting of Dock3 may regulate the intracellular localization of WAVE. To assess this possibility, we transfected SY5Y cells with WT Dock3 and subjected them to immunocytochemistry. Overexpression of WT Dock3 did not change the intracellular localization of WAVE1 (Fig. 4*F*). In contrast, overexpression of farnesylated Dock3 (F-Dock3, a membrane-targeted form of Dock3) translocated WAVE1 from the cytoplasm to the peripheral regions (arrowheads in Fig. 4*F*). Taken together, these results suggest that the DHR-1 domain of Dock family proteins mediates direct binding to WAVE proteins leading to colocalization at the cell periphery and axonal outgrowth.

We also found a strong enhancement of the Dock3 upper mobility band (arrow in Fig. 4*G*) in Cos-7 cells transfected with F-Dock3 but not with WT Dock3 (26 ± 6% and 2 ± 1% of total Dock3, respectively). Consistent with the upper mobility band representing a phosphorylated form of Dock3, the mobility shift was eliminated by phosphatase treatment (Fig. 4*G*). We next examined the effect of Dock3 phosphorylation on its ability to bind WAVE. Cos-7 cells were transfected with His-tagged WAVE1 and F-Dock3 and subjected to a pull-down assay. Immunoblot analysis revealed that WAVE1 binds to the unphosphorylated form of Dock3 more effectively than to the phosphorylated form (Fig. 4*H*). Thus, the Dock3/WAVE1 complex may dissociate upon Dock3 phosphorylation, leading to spatially restricted actin dynamics through WAVE signaling.

Promoting Axonal Outgrowth in Adult CNS by Modulating Dock3 Activity. To investigate the effects of Dock3 in vivo, we generated transgenic (Tg) mice overexpressing WT Dock3 under control of the actin promoter. Tg mice showed high expression levels of Dock3 in many tissues, especially in the optic nerve (~5.6-fold) and retina (~2.3-fold; Fig. S6*A*), but the structure of such tissues were normal (Fig. S6 *B* and *C*). Therefore, we prepared retinal explants from WT and Tg mice and examined the effect of Dock3 on axon length. Quantitative analysis revealed that axon length was clearly greater in Tg mice than in their WT littermates (Fig. 5*A*). Furthermore, Dock3 and BDNF exerted synergistic effects on axonal growth, as observed in vitro (Fig. 2 *A* and *B*). These results suggest that axonal outgrowth is promoted in Dock3 Tg mice. To explore this possibility, we used the optic nerve microcrush model and investigated the extent of axonal outgrowth 2 weeks after injury by staining with GAP43 antibody (22). WT mice subjected to nerve crush showed >40 axons extending 200 μm from the injury site, and half this number extended 500 μm. In contrast, Tg mice had, on average, >80 axons extending 200 μm and >60 axons extending 500 μm beyond the lesion site (Fig. 5*B*). Immunohistochemical analysis of Dock3 and WAVE1 in injured optic nerves revealed that their coexpression was hardly detectable in WT mice, but was clearly increased in regenerating axons in Tg mice (Fig. 5*C*). We next examined the levels of Dock3 and WAVE1 proteins in optic nerves by immunoblotting (Fig. S7). Dock3 protein was reduced in injured WT optic nerves (decreased to ~10% of control), but this reduction was less severe in Tg mice. In both WT and Tg mice, WAVE1 protein was less abundant after the injury (reduced to ~60%). Whereas in the membrane fraction of crushed optic nerves, Dock3 and WAVE1 expression levels in Tg mice were significantly higher than WT mice (Fig. 5*D* and *E*). We also examined the expression of TrkB and Fyn in injured optic nerves, but their expression levels in Tg mice were not significantly altered compared with those in WT mice (Fig. S8). Thus, overexpression of Dock3 does not affect the expression levels of its binding partners, but may induce axonal outgrowth through effective membrane recruitment of WAVE1.

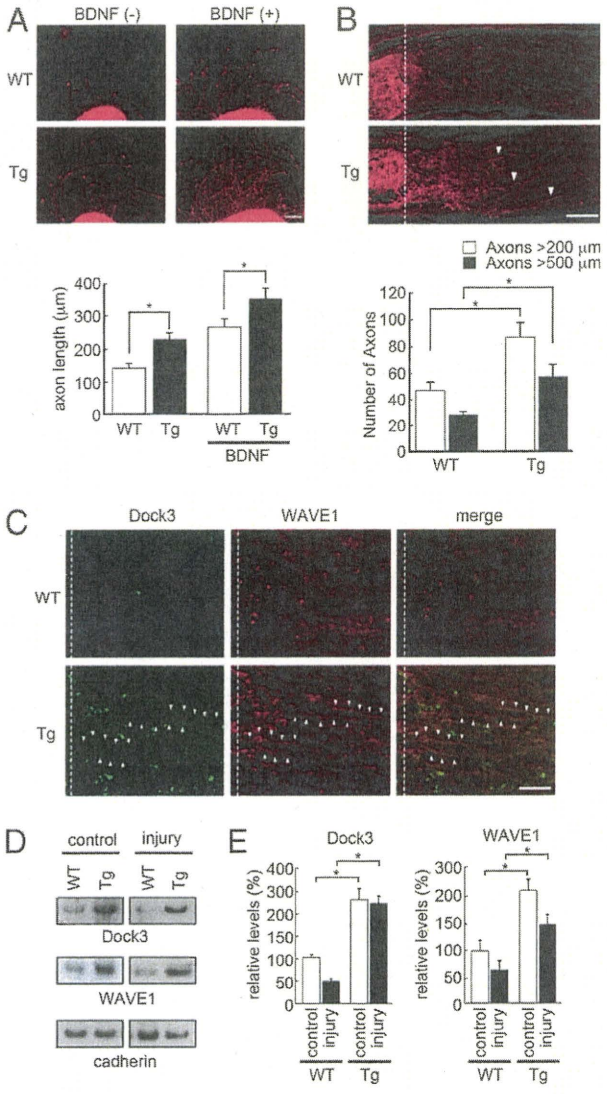

Fig. 5. Overexpression of Dock3 induces axonal regeneration in vivo. (*A*) (*Upper*) Retinal explants from WT and Dock3 Tg mice cultured in the presence or absence of BDNF were fixed and labeled with phalloidin at 2 days in vitro. (*Lower*) Axon length was measured and quantified. Data are mean ± SEM, $n > 80$ axons for each group. $^*P < 0.05$. (Scale bar, 100 μm.) (*B*) (*Upper*) GAP43-labeled axons in the optic nerve proximal to the injury site (dotted line) 2 weeks after nerve surgery. Arrowheads indicate regenerating axons. (*Lower*) Regenerating axons from lesion site were measured and quantified. Data are mean ± SEM for six independent experiments. $^*P < 0.05$. (Scale bar, 50 μm.) (*C*) Immunostaining of the optic nerves proximal to the injury site (dotted line). Arrowheads indicate colocalization of Dock3 (green) and WAVE1 (red) in the regenerating axons. (Scale bar, 20 μm.) (*D*) Immunoblot analysis of Dock3 and WAVE1 in the membrane fraction of optic nerve 2 weeks after nerve surgery. (*E*) Expression levels of Dock3 and WAVE1 in the membrane fraction of normal and injured optic nerves were quantified. Data are presented as means ± SEM of three independent experiments. $^*P < 0.05$.

Discussion

In the present study, we found that Dock1–4, which are atypical members of the Rho-GEF family, share several conserved amino acids in their DHR-2 domains that are required for GEF activity. In addition, Dock1–4 bind directly to WAVE1–3 via their DHR-1 domains, and this is disrupted when Dock1–4 become phosphorylated. We further showed that Dock3 forms a protein complex with Fyn and WAVE1 at the plasma membrane downstream of TrkB. Finally, we demonstrated that overexpression of Dock3 increases WAVE1 expression levels in the plasma membrane

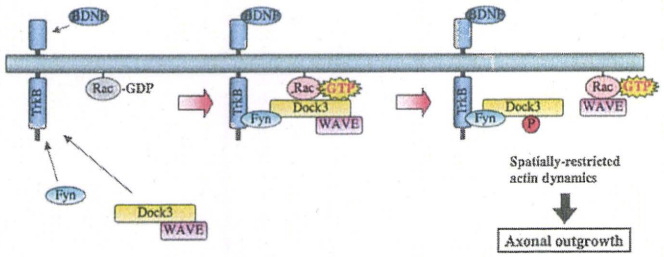

Fig. 6. Proposed role of Dock3 in BDNF-mediated axonal outgrowth. BDNF-TrkB signaling induces Fyn phosphorylation and stimulates membrane recruitment of the Dock3/WAVE complex. Dock3 is then able to activate Rac-GDP (inactive form). Rac-GTP (active form) and WAVE are dissociated from phosphorylated Dock3 and stimulate actin reorganization, leading to axonal outgrowth.

and promotes optic nerve regeneration in vivo. Taken together, our results suggest a unique mechanism for axonal outgrowth through which Dock-GEFs recruit WAVE proteins to specific sites within cells and induce spatially restricted actin dynamics in the CNS (Fig. 6).

BDNF/TrkB signaling is important for a variety of CNS developmental processes including synaptic pruning (23, 24). In addition, Rho-GTPase signaling can affect both spine structure and synaptic function (25, 26). In this study, we found that treatment of hippocampal neurons with BDNF enhances Rac1 activation and neurite outgrowth. It is therefore possible that Dock-GEFs mediate multiple BDNF/TrkB functions, including the establishment of long-term potentiation. On the other hand, loss of Dock3 leads to sensorimotor impairments and structural changes, including axonal swellings, but had no effects on life span or fertility (15). These relatively mild phenotypes are reasonable, considering the redundant catalytic sequences found in the DHR-2 domains of Dock1–4. Recent studies have revealed that a Val66Met polymorphism in human BDNF is involved in the pathogenesis of attention-deficit/hyperactivity disorder (ADHD) (27–29). Interestingly, a pericentric inversion breakpoint in the *DOCK3* gene has been described in ADHD patients (30). Thus, further study is required to determine the full implications of the Dock-GEFs in BDNF-associated development, adult physiology, and disease.

Dock3 overexpression induced optic nerve regeneration after injury without affecting expression levels of its binding partners. For example, WAVE1 expression level after optic nerve injury was decreased to ~60% in both WT and Dock3 Tg mice. However, WAVE1 expression was increased in the membrane fraction and was coexpressed with Dock3 in the regenerating axons. Thus, the tight regulation of Rac1-GDP/Rac1-GTP cycling and effective membrane recruitment of WAVE proteins by Dock3, rather than prolonged activation of Rac1 or WAVE proteins (31–33), may be required for axonal growth via actin polymerization. Our present findings support the notion that neurons have to intrinsically upregulate the necessary growth-associated molecules to extend an axon (34, 35). On the other hand, recent studies have shown that glial scarring and several myelin inhibitors block axonal growth following CNS injury (35, 36). Thus, overexpression of Dock-GEFs may have a synergistic effect in combination with suppression of glial scarring and myelin-associated inhibitory signaling.

Lack of axonal regeneration in the adult CNS is one of the most important issues to be resolved in various neurodegenerative disorders. For example, glaucoma is characterized by a slow progressive degeneration of optic nerve axons. Thus, Dock/WAVE complexes and their related binding partners may be possible therapeutic targets in multiple forms of glaucoma that otherwise lead to severe visual impairment. We are presently investigating these issues by crossing Dock3 Tg mice with glutamate transporter knockout mice, which are the first animal models of normal tension glaucoma (37). Thus, further studies are required to explore the full potential of Dock-GEFs that could be used for effective regeneration therapy.

Materials and Methods

Experimental Animals. Experiments were performed using $p75^{NTR}$ knockout and TrkB × hGFAP-cre knockout (TrkB KO) mice in accordance with the Tokyo Metropolitan Institute for Neuroscience *Guidelines for the Care and Use of Animals*. The TrkB deletion was confirmed in the hippocampus of the TrkB KO mice (23). A Tg construct containing the CAG promoter, *Dock3* coding sequence (GenBank accession no. NM_153413), and a poly-adenylation signal was used to generate Dock3 Tg mice. The founder mice were generated by injecting the transgene into fertilized C57BL/6 eggs. RGCs were retrogradely labeled with Fluoro-Gold (Fluorochrome) as previously described (38).

Cell Culture. Primary cultured hippocampal neurons (39) and retinal explants (22) were prepared from E16 mice. In some experiments, they were stimulated with BDNF (5 or 50 ng/mL; Alomone Labs).

Plasmids and siRNA Transfection. WAVE1–3 plasmids were provided by T. Takenawa (40). Elmo2 and GST-CRIB plasmids were provided by H. Kato and M. Negishi (21). Rac and Dock1 plasmids were provided by M. Matsuda (41). Dock3, Fyn, and WAVE1 fragments were PCR-amplified from full-length cDNAs and expressed as His-tagged proteins. Alanine substitutions were generated with the PrimeSTAR Mutagenesis Basal Kit (Takara). RNA oligomers containing 21 nucleotides for RNA interference for Dock1–4 were synthesized in the sense and antisense directions (Dock1: 5′-GGAAGUCACCACAACGCU UUU-3′; Dock2: 5′-GCAUCUCA CGCUACAGAUUUU-3′; Dock3: 5′-GCAGAUCA GUGAACGGUUUU-3′; Dock4: 5′-GCAAGAGUGUGGCCAGAAAUU-3′) (JBioS). Transfection of siRNAs and plasmids was performed using the Nucleofector System (Amaxa) or Lipofectamine Plus (Invitrogen).

Pull-Down Assay. His-tagged proteins were purified from Cos-7 cell lysates with TALON resin (BD Biosciences) for 20 min at 4 °C with gentle agitation. The protein levels of Rac-GTP were measured by affinity precipitation using the GST-CRIB of PAK1. Bacterial GST-fusion proteins were incubated with lysates from Cos-7 cells or mouse brains. The precipitated samples were subjected to SDS-PAGE followed by immunoblot analysis (8) with the following antibodies: Fyn, phospho-Fyn (Tyr416) and WAVE1 were obtained from BD Biosciences; WAVE2 and WAVE3 were obtained from Santa Cruz.

Immunostaining. SY5Y cells, retinal explants, sections of retina, and optic nerves were incubated with anti-Dock3 (1:200), anti-WAVE1 (1:200), and anti-GAP43 (1:1,000; Chemicon) antibodies. Cy2-conjugated donkey antirabbit IgG or Cy3-conjugated donkey antimouse IgG were used as secondary antibodies. F-actin was visualized with rhodamine-labeled phalloidin (Invitrogen).

Optic Nerve Injury. Mice were anesthetized with sodium pentobarbital before optic nerve crush. Optic nerves were exposed intraorbitally and crushed about 0.5–1.0 mm from the posterior pole of the eyeball with fine surgical forceps for 5 s (22). Fourteen days after surgery, axonal outgrowth was quantified by counting GAP43-positive axons that crossed a virtual line parallel to the lesion site at 200 μm and 500 μm distal to the lesion site. Protein expression levels in the lesion site were measured by immunoblot analysis with antibodies against Dock3 and WAVE1–3. Membrane fraction was prepared as previously described (42).

Image Analysis and Statistics. To measure axon length, the longest axon of each neuron was traced and calculated using National Institutes of Health ImageJ (version 1.38). Approximately 50 neurons with axons were scanned using a DP70 CCD camera (Olympus). Data are presented as mean ± SEM. For statistical analyses, a two-tailed Student's *t* test was used. Values of $P < 0.05$ were regarded as statistically significant.

ACKNOWLEDGMENTS. We are grateful to T. Takenawa (Kobe University) and H. Kato, M. Negishi, and M. Matsuda (Kyoto University) for reagents. We thank A. Kimura, K. Nakamura, and K. Nishimura for technical assistance, and R. McKay for comments on the manuscript. This study was supported by grants from the Ministry of Education, Culture, Sports, Science and Technology of Japan (to K.N., C.H., and T.H.); Ministry of Health, Labour, and Welfare of Japan; Uehara Memorial Foundation; Naito Foundation; Suzuken Memorial Foundation; Daiwa Securities Health Foundation; Takeda Science Foundation; and Japan Medical Association (to T.H.).

1. Iwasato T, et al. (2007) Rac-GAP alpha-chimerin regulates motor-circuit formation as a key mediator of EphrinB3/EphA4 forward signaling. *Cell* 130:742–753.
2. Schmidt A, Hall A (2002) Guanine nucleotide exchange factors for Rho GTPases: Turning on the switch. *Genes Dev* 16:1587–1609.
3. Goley ED, Welch MD (2006) The ARP2/3 complex: An actin nucleator comes of age. *Nat Rev Mol Cell Biol* 7:713–726.
4. Takenawa T, Suetsugu S (2007) The WASP-WAVE protein network: Connecting the membrane to the cytoskeleton. *Nat Rev Mol Cell Biol* 8:37–48.
5. Cerione RA, Zheng Y (1996) The Dbl family of oncogenes. *Curr Opin Cell Biol* 8:216–222.
6. Lemmon MA, Ferguson KM (2000) Signal-dependent membrane targeting by pleckstrin homology (PH) domains. *Biochem J* 350:1–18.
7. Côté JF, Vuori K (2002) Identification of an evolutionarily conserved superfamily of DOCK180-related proteins with guanine nucleotide exchange activity. *J Cell Sci* 115: 4901–4913.
8. Namekata K, Enokido Y, Iwasawa K, Kimura H (2004) MOCA induces membrane spreading by activating Rac1. *J Biol Chem* 279:14331–14337.
9. Guan KL, Rao Y (2003) Signalling mechanisms mediating neuronal responses to guidance cues. *Nat Rev Neurosci* 4:941–956.
10. Harada T, Harada C, Parada LF (2007) Molecular regulation of visual system development: More than meets the eye. *Genes Dev* 21:367–378.
11. Harada T, et al. (2000) Modification of glial-neuronal cell interactions prevents photoreceptor apoptosis during light-induced retinal degeneration. *Neuron* 26: 533–541.
12. Segal RA (2003) Selectivity in neurotrophin signaling: Theme and variations. *Annu Rev Neurosci* 26:299–330.
13. Knapp D, Messenger N, Ahmed Rana A, Smith JC (2006) Neurotrophin receptor homolog (NRH1) proteins regulate mesoderm formation and apoptosis during early Xenopus development. *Dev Biol* 300:554–569.
14. Passino MA, Adams RA, Sikorski SL, Akassoglou K (2007) Regulation of hepatic stellate cell differentiation by the neurotrophin receptor p75NTR. *Science* 315:1853–1856.
15. Chen Q, et al. (2009) Loss of modifier of cell adhesion reveals a pathway leading to axonal degeneration. *J Neurosci* 29:118–130.
16. Kunisaki Y, et al. (2006) DOCK2 is a Rac activator that regulates motility and polarity during neutrophil chemotaxis. *J Cell Biol* 174:647–652.
17. Laurin M, et al. (2008) The atypical Rac activator Dock180 (Dock1) regulates myoblast fusion in vivo. *Proc Natl Acad Sci USA* 105:15446–15451.
18. Miyamoto Y, Yamauchi J, Tanoue A, Wu C, Mobley WC (2006) TrkB binds and tyrosine-phosphorylates Tiam1, leading to activation of Rac1 and induction of changes in cellular morphology. *Proc Natl Acad Sci USA* 103:10444–10449.
19. Pereira DB, Chao MV (2007) The tyrosine kinase Fyn determines the localization of TrkB receptors in lipid rafts. *J Neurosci* 27:4859–4869.
20. Davidson D, Chow LM, Fournel M, Veillette A (1992) Differential regulation of T cell antigen responsiveness by isoforms of the src-related tyrosine protein kinase p59fyn. *J Exp Med* 175:1483–1492.
21. Katoh H, Negishi M (2003) RhoG activates Rac1 by direct interaction with the Dock180-binding protein Elmo. *Nature* 424:461–464.
22. Fischer D, He Z, Benowitz LI (2004) Counteracting the Nogo receptor enhances optic nerve regeneration if retinal ganglion cells are in an active growth state. *J Neurosci* 24:1646–1651.
23. Luikart BW, et al. (2005) TrkB has a cell-autonomous role in the establishment of hippocampal Schaffer collateral synapses. *J Neurosci* 25:3774–3786.
24. Zhou Z, et al. (2006) Brain-specific phosphorylation of MeCP2 regulates activity-dependent Bdnf transcription, dendritic growth, and spine maturation. *Neuron* 52: 255–269.
25. Nakayama AY, Harms MB, Luo L (2000) Small GTPases Rac and Rho in the maintenance of dendritic spines and branches in hippocampal pyramidal neurons. *J Neurosci* 20:5329–5338.
26. Tashiro A, Yuste R (2004) Regulation of dendritic spine motility and stability by Rac1 and Rho kinase: Evidence for two forms of spine motility. *Mol Cell Neurosci* 26: 429–440.
27. Egan MF, et al. (2003) The BDNF val66met polymorphism affects activity-dependent secretion of BDNF and human memory and hippocampal function. *Cell* 112:257–269.
28. Friedel S, et al. (2005) Mutation screen of the brain derived neurotrophic factor gene (BDNF): Identification of several genetic variants and association studies in patients with obesity, eating disorders, and attention-deficit/hyperactivity disorder. *Am J Med Genet B Neuropsychiatr Genet* 132B:96–99.
29. Kent L, et al. (2005) Association of the paternally transmitted copy of common Valine allele of the Val66Met polymorphism of the brain-derived neurotrophic factor (BDNF) gene with susceptibility to ADHD. *Mol Psychiatry* 10:939–943.
30. de Silva MG, et al. (2003) Disruption of a novel member of a sodium/hydrogen exchanger family and DOCK3 is associated with an attention deficit hyperactivity disorder-like phenotype. *J Med Genet* 40:733–740.
31. Kawano Y, et al. (2005) CRMP-2 is involved in kinesin-1-dependent transport of the Sra-1/WAVE1 complex and axon formation. *Mol Cell Biol* 25:9920–9935.
32. Luo L, Jan LY, Jan YN (1997) Rho family GTP-binding proteins in growth cone signalling. *Curr Opin Neurobiol* 7:81–86.
33. Zipkin ID, Kindt RM, Kenyon CJ (1997) Role of a new Rho family member in cell migration and axon guidance in C. elegans. *Cell* 90:883–894.
34. Bouquet C, Nothias F (2007) Molecular mechanisms of axonal growth. *Adv Exp Med Biol* 621:1–16.
35. Hannila SS, Filbin MT (2008) The role of cyclic AMP signaling in promoting axonal regeneration after spinal cord injury. *Exp Neurol* 209:321–332.
36. Cafferty WB, McGee AW, Strittmatter SM (2008) Axonal growth therapeutics: Regeneration or sprouting or plasticity? *Trends Neurosci* 31:215–220.
37. Harada T, et al. (2007) The potential role of glutamate transporters in the pathogenesis of normal tension glaucoma. *J Clin Invest* 117:1763–1770.
38. Harada C, et al. (2006) Role of apoptosis signal-regulating kinase 1 in stress-induced neural cell apoptosis in vivo. *Am J Pathol* 168:261–269.
39. Yoshimura T, et al. (2005) GSK-3beta regulates phosphorylation of CRMP-2 and neuronal polarity. *Cell* 120:137–149.
40. Oda A, et al. (2005) WAVE/Scars in platelets. *Blood* 105:3141–3148.
41. Kiyokawa E, et al. (1998) Activation of Rac1 by a Crk SH3-binding protein, DOCK180. *Genes Dev* 12:3331–3336.
42. Nakamura K, Namekata K, Harada C, Harada T (2007) Intracellular sortilin expression pattern regulates proNGF-induced naturally occurring cell death during development. *Cell Death Differ* 14:1552–1554.

Supporting Information

Namekata et al. 10.1073/pnas.0914514107

SI Materials and Methods

Hippocampal Neuron Cultures. Primary cultures of mouse hippocampal neurons were prepared as described previously (1). Briefly, 16-day-old mouse embryos were killed by decapitation, and the hippocampi were dissected in L-15 medium, treated with (0.25% trypsin, 0.5% glucose, and 1% DNase I in PBS for 30 min, washed, and dissociated by pipetting. The resulting dissociated hippocampal neurons were plated on a poly-D-lysine–coated cover glass. Neurons were cultured in DMEM containing 10% FCS for 3 h and then cultured in DMEM supplemented with B27 for 3 days. In some experiments, neurons were stimulated with BDNF (5 or 50 ng/mL; Alomone Labs) and K252a (200 ng/mL; Alomone Labs).

Immunostaining of the Retina. Immunohistochemical analysis of the retina was carried out as previously reported (2). Briefly, retinal sections were incubated overnight with a rabbit polyclonal antibody against Dock3, a goat polyclonal antibody against Brn3b (Santa Cruz), or mouse monoclonal antibodies against calretinin (Chemicon), calbindin (Sigma) or glutamine synthetase (GS; Chemicon). These antibodies were then visualized with a DAKO Envision kit (DAKO), Cy3-conjugated donkey antirabbit IgG, Cy2-conjugated donkey antigoat IgG, or FITC-conjugated donkey antimouse IgG (Jackson Immunoresearch).

Histological and Immunoblot Analysis of Optic Nerves. Optic nerve sections were stained with luxol fast blue (LFB) followed by H&E. For detailed morphological analysis, optic nerves were fixed in 2% glutaraldehyde and 2% paraformaldehyde in 0.1 M phosphate buffer overnight at 4 °C. After dissection, the pieces of tissue were placed in 1% osmium tetroxide. After dehydration, the pieces were embedded in EPON (Nisshin EM, Tokyo, Japan). Transverse semithin (500 nm) sections were stained with 0.2% toluidine blue in 1.0% sodium borate (3). Glial scars were labeled with anti-GFAP antibody (Progen) 3 and 14 days after injury.

1. Yoshimura T, et al. (2005) GSK-3β regulates phosphorylation of CRMP-2 and neuronal polarity. *Cell* 120:137–149.
2. Harada C, et al. (2006) Effect of p75NTR on the regulation of naturally occurring cell death and retinal ganglion cell number in the mouse eye. *Dev Biol* 290:57–65.
3. Harada T, et al. (2007) The potential role of glutamate transporters in the pathogenesis of normal tension glaucoma. *J Clin Invest* 117:1763–1770.

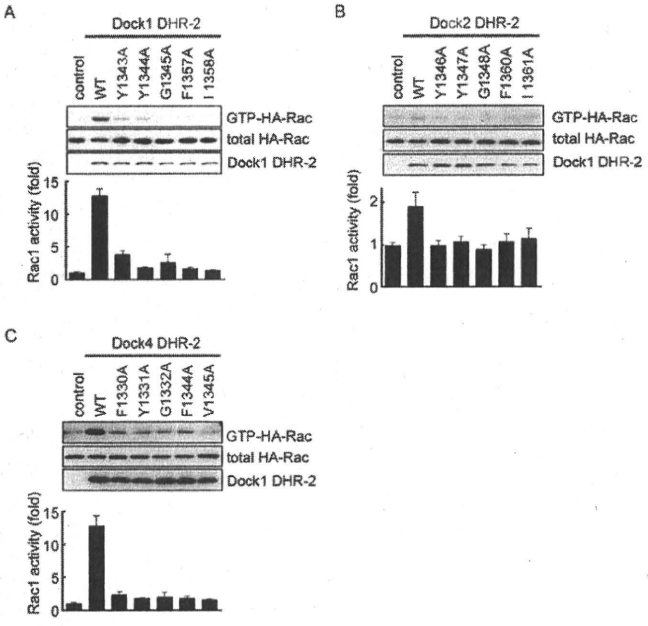

Fig. S1. Identification of critical residues for catalytic activity in the DHR-2 domain of Dock1, Dock2, and Dock4. Cos-7 cells were transfected with the indicated alanine-substitution mutants of Dock1 (*A*), Dock2 (*B*), and Dock4 (*C*). Lysates were subjected to a GST-CRIB assay.

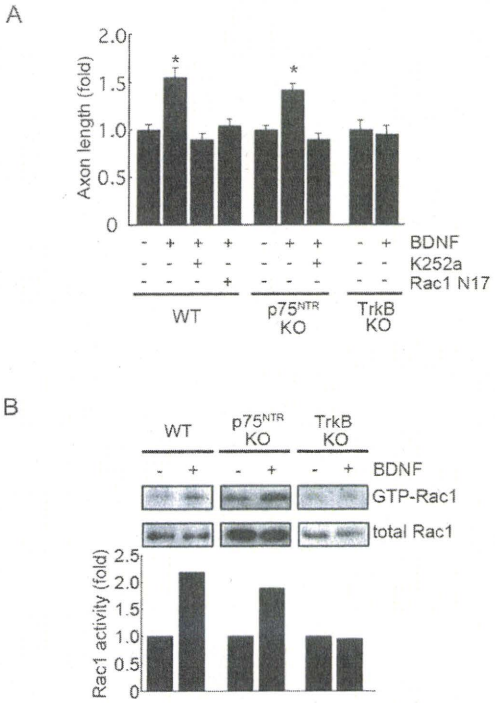

Fig. S2. BDNF-mediated axonal outgrowth and Rac1 activation via TrkB. (*A*) Hippocampal neurons from WT, $p75^{NTR}$ KO, or TrkB KO mice were transfected with GFP and treated as shown at the *x* axis. Axon length was measured at 3 days in vitro (DIV). $n = 30$ for each experimental condition. Data are mean ± SEM of three independent experiments. $*P < 0.05$. (*B*) Lysates of hippocampal neurons from WT, $p75^{NTR}$ KO, or TrkB KO mice were subjected to a GST-CRIB assay. Quantitation of GTP-Rac is shown underneath.

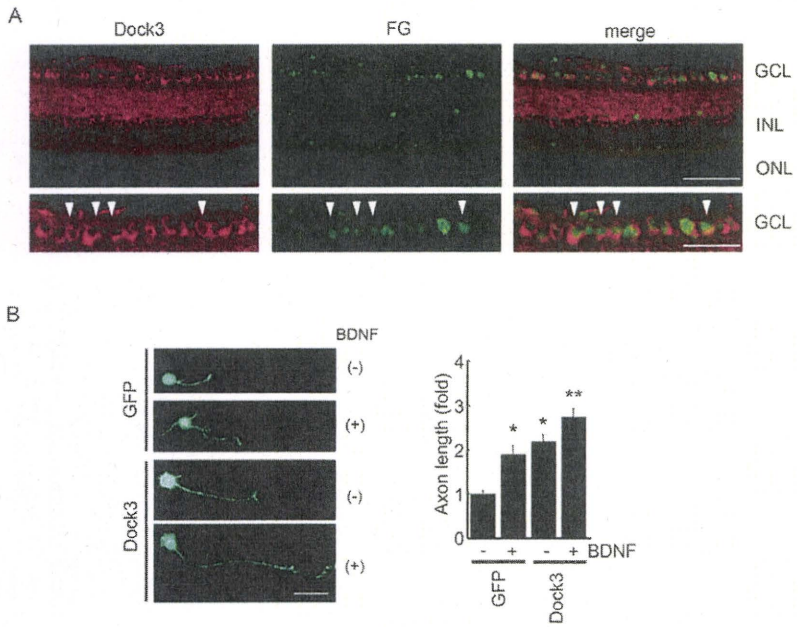

Fig. S3. Dock3 enhances BDNF-mediated axonal outgrowth in RGCs. (*A*) Dock3 expression in the retina. Dock3 was detected in Fluoro-Gold (FG)–labeled retinal ganglion cells (arrows). Scale bars, 50 μm in the upper row and 25 μm in the lower row. (*B*) (*Left*) RGCs were transfected with GFP alone or with GFP and Dock3 and then cultured in the presence or absence of BDNF for 3 days. (Scale bar, 20 μm.) (*Right*) RGCs transfected and treated as shown at the *x* axis were fixed at 3 days *in vitro*, and axon length was measured. $n = 50$ for each experimental condition. Data are mean ± SEM of three independent experiments. $*P < 0.05$, $**P < 0.01$.

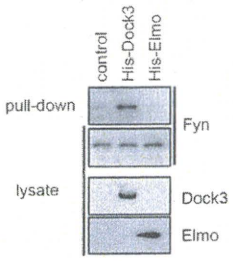

Fig. S4. Fyn binds to Dock3 but not to Elmo. Lysates from Cos-7 cells transfected with Fyn^{Y528F} and either His-tagged Dock3 or His-tagged, Elmo were subjected to His-tag pull-down assays. Precipitates were detected with antibodies against Fyn, Dock3, and Elmo.

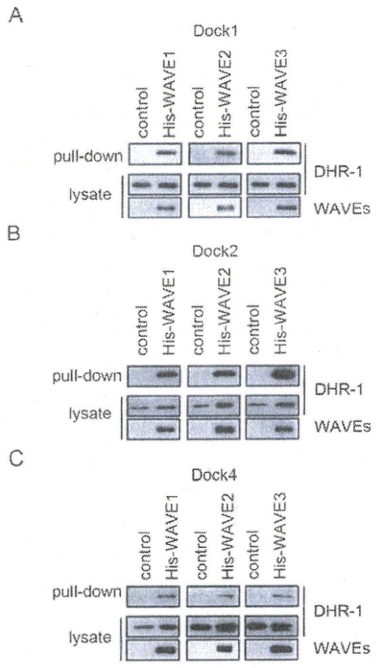

Fig. S5. Direct binding of Dock family members and WAVE proteins. Lysates from Cos-7 cells transfected with the myc-DHR-1 domain of Dock1 (*A*), Dock2 (*B*), or Dock4 (*C*) and His-tagged WAVE1, WAVE2, or WAVE3 were subjected to His-tag pull-down assays with antibodies against myc-tag, WAVE1, WAVE2, and WAVE3.

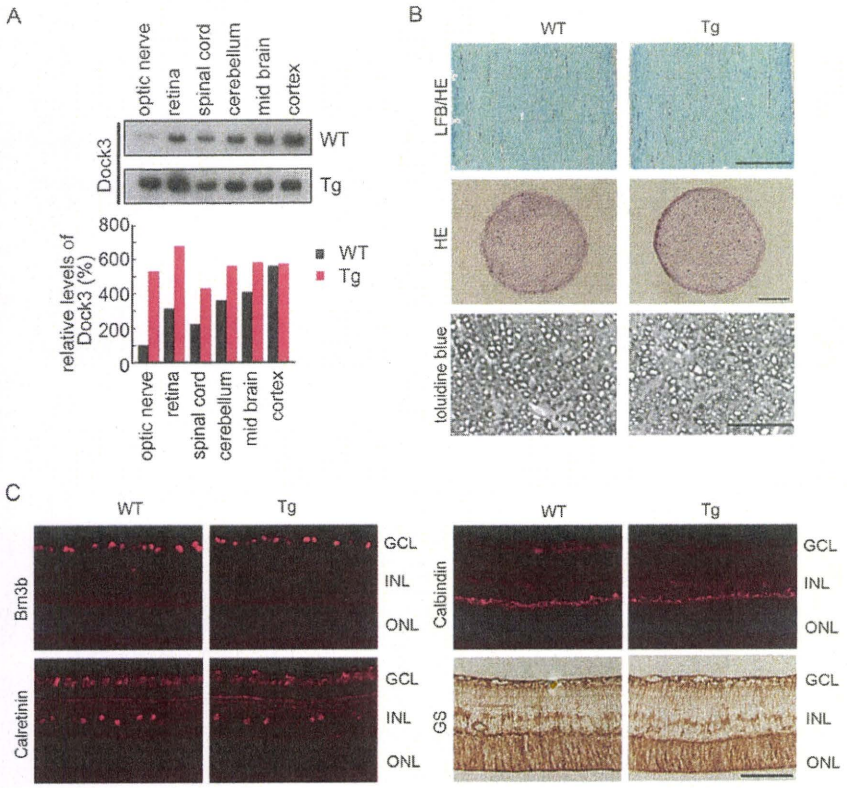

Fig. S6. Histological analysis of adult optic nerves and retina in Dock3 Tg mice. (*A*) Immunoblot analysis of various tissues from WT and Tg mice. Quantifications of Dock3 are shown underneath. (*B*) Histological analysis of optic nerves in WT and Dock3 Tg mice. (*Upper*) Staining with luxol fast blue (LFB) and hematoxylin and eosin (HE). (*Middle*) Transverse sections stained with H&E. (*Lower*) Semithin transverse sections stained with toluidine blue. [Scale bar, 100 μm (*Upper*) and 20 μm (*Middle* and *Lower*).] (C) Immunohistochemical analysis of Brn3b (RGCs), calretinin (RGCs and amacrine cells), calbindin (horizontal cells), glutamine synthetase (GS; Müller cells) in WT and Dock3 Tg mice. Data show no apparent difference between WT and Tg mice. GCL, ganglion cell layer; INL, inner nuclear layer; ONL, outer nuclear layer. (Scale bar, 50 μm.)

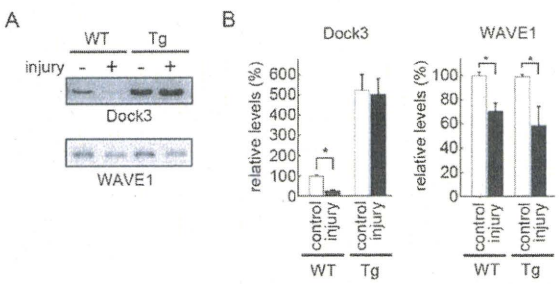

Fig. S7. Expression levels of total Dock3 and WAVE1 in injured optic nerves. (*A*) Immunoblot analysis of optic nerve proteins using antibodies against Dock3 and WAVE1. (*B*) Expression levels of total Dock3 and WAVE1 in normal and injured optic nerves were quantified. Data are mean ± SEM of three independent experiments. $*P < 0.05$.

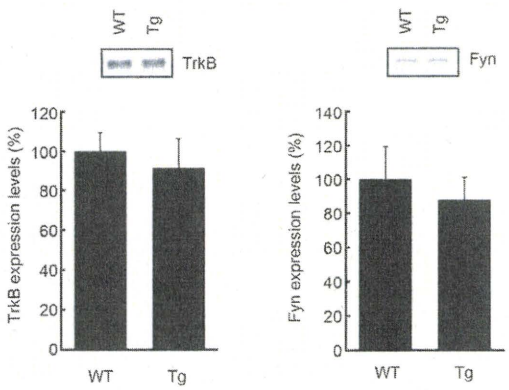

Fig. S8. Expression levels of TrkB and Fyn in injured optic nerves. Immunoblot analysis of optic nerve proteins from injured WT and Dock3 Tg mice (*Upper*). Data show no apparent difference between WT and Tg mice. Expression levels of TrkB and Fyn are shown as mean ± SEM of three independent experiments (*Lower*).

J Neuropathol Exp Neurol

Vol. 69, No. 7
July 2010
pp. 667–676

ORIGINAL ARTICLE

Aberrant Detergent-Insoluble Excitatory Amino Acid Transporter 2 Accumulates in Alzheimer Disease

Randall L. Woltjer, MD, PhD, Kevin Duerson, PhD, Joseph M. Fullmer, MD, PhD, Paramita Mookherjee, PhD, Allison M. Ryan, Thomas J. Montine, MD, PhD, Jeffrey A. Kaye, MD, Joseph F. Quinn, MD, Lisa Silbert, MD, MCR, Deniz Erten-Lyons, MD, James B. Leverenz, MD, Thomas D. Bird, MD, David V. Pow, PhD, Kohichi Tanaka, MD, PhD, G. Stennis Watson, PhD, and David G. Cook, PhD

Abstract

Alzheimer disease (AD) is characterized by deposition of amyloid-β, tau, and other specific proteins that accumulate in the brain in detergent-insoluble complexes. Alzheimer disease also involves glutamatergic neurotransmitter system disturbances. Excitatory amino acid transporter 2 (EAAT2) is the dominant glutamate transporter in cerebral cortex and hippocampus. We investigated whether accumulation of detergent-insoluble EAAT2 is related to cognitive impairment and neuropathologic changes in AD by quantifying detergent-insoluble EAAT2 levels in hippocampus and frontal cortex of cognitively normal patients, patients with clinical dementia rating of 0.5 (mildly impaired), and AD patients. Parkinson disease patients served as neurodegenerative disease controls. We found that Triton X-100–insoluble EAAT2 levels were significantly increased in patients with AD compared with controls, whereas Triton X-100–insoluble EAAT2 levels in patients with clinical dementia rating of 0.5 were intermediately elevated between control and AD subjects. Detergent insolubility of presenilin-1, a structurally similar protein, did not differ among the groups, thus arguing that EAAT2 detergent insolubility was not caused by nonspecific cellular injury. These findings demonstrate that detergent-insoluble EAAT2 accumulation is a progressive biochemical lesion that correlates with cognitive impairment and neuropathologic changes in AD. These findings lend further support to the idea that dysregulation of the glutamatergic system may play a significant role in AD pathogenesis.

Key Words: Glutamate, Alzheimer disease, EAAT2, Excitotoxicity, Mild cognitive impairment, Protein aggregation, Oxidative stress, SLC1A2.

From the Department of Pathology (RLW, AMR), Oregon Health & Sciences Univ., Portland, Oregon; Geriatric Research Education and Clinical Center (KD, TDB, SW, DGC), VA Medical Center (VAPSHCS), Seattle, Washington; Department of Pathology (JMF), University of Wisconsin, Madison, Wisconsin; Department of Pathology (PM, TJM), University of Washington, Seattle, Washington; Department of Neurology (JAK, JFQ, LS, DE-L), Oregon Health & Sciences University, Portland, Oregon; Research and Development Service (DE-L), VA Medical Center, Portland, Oregon; Department of Neurology (JBL, TDB), University of Washington, Seattle, Washington; U.Q. Centre for Clinical Research (DVP), Royal Brisbane and Women's Hospital, Brisbane, Australia; Laboratory of Molecular Neuroscience (KT), School of Biomedical Science and Medical Research Institute, Tokyo Medical and Dental University, Tokyo, Japan; Department of Psychiatry and Behavioral Sciences (GSW), University of Washington, Seattle, Washington; and Departments of Medicine and Pharmacology (DGC), University of Washington, Seattle, Washington.

Send correspondence and reprint requests to: David G. Cook, PhD, VA Medical Center, Geriatric Research Education and Clinical Center, 1660 S. Columbian Way, Seattle, WA 98108; E-mail: dgcook@u.washington.edu

This study was supported by the Veteran's Affairs Office of Research and Development Medical Research Service (David Cook); by NIH institutional fellowships to Kevin Duerson, Joseph Fullmer (T32 AG000258), and Paramita Mookherjee (T32 AG00057-31); by the University of Washington Alzheimer's Disease Research Center (AG5036); and by the Oregon Alzheimer's Disease Center (5P30AG008017).

INTRODUCTION

Aberrant glutamate stimulation has been proposed as a mechanism by which synapses and neurons are injured in Alzheimer disease (AD) (1). Excitatory amino acid transporter 2 ([EAAT2] also called *GLT-1*) is the major glutamate transporter in the forebrain that is responsible for a number of essential neuroprotective and regulatory functions that include preventing glutamate-mediated injury to neurons and synapses and regulating normal synaptic input specificity (2–5). Several reports indicate that EAAT2 levels are significantly reduced in AD (6–8), thus raising the possibility that glutamate dyshomeostasis plays a role in AD pathogenesis. In addition, EAAT2 is oxidatively damaged by exposure to amyloid-β (Aβ) (9–13). Excitatory amino acid transporter 2 oxidation impairs glutamate uptake and promotes the formation of high–molecular weight EAAT2 oligomers that are insoluble in detergents such as Triton X-100 (14–16).

These findings suggest that AD pathogenesis may disrupt EAAT2 via mechanisms that recapitulate those of other key AD-related molecules, most notably Aβ, which undergoes oxidation, misfolding, and aggregation. Although the studies previously cited establish that EAAT2 is biochemically and functionally damaged by Aβ-related processes, the potential disease relevance of these findings has not been examined in AD patients. There currently is little evidence at the protein level on the relationship between aberrant EAAT2 expression and the degree of cognitive loss and associated AD pathology. To address this important issue, we measured Triton X-100–insoluble and Triton X-100–soluble

EAAT2 in the hippocampus and frontal cortex of more than 100 clinically and pathologically well-characterized normal controls, patients with a Clinical Dementia Rating (CDR) of 0.5 (17), and later-stage AD patients.

MATERIALS AND METHODS

Patients

Subjects were from the Alzheimer's Disease Center, Oregon Health and Sciences University, and Alzheimer's Disease Research Center at the University of Washington (Table). Control subjects and subjects with a CDR = 0.5 (intended to approximate mild cognitive impairment) were participants in brain aging studies at the Oregon Aging/Alzheimer's Disease Center. Subjects received annual neurological and neuropsychological evaluation, with CDR assigned by an experienced clinician. Controls had normal cognitive and functional examinations. Subjects with a CDR = 0.5 were functionally intact on enrollment and progressed to a global CDR = 0.5 (no subscores >0.5) at their last evaluation, within a year of autopsy. The AD subjects were diagnosed by a clinical team consensus conference, met National Institute for Neurological and Communicative Disorders and Stroke-Alzheimer's Disease and Related Disorder Association diagnostic criteria for clinical AD, had a CDR of greater than 1.0, and neuropathologic confirmation at autopsy (after informed consent). Tissue use conformed to institutional review board–approved protocols. Neuropathologic assessment conformed to National Institute on Aging–Reagan consensus criteria (18). The AD group included subjects with probable AD, moderate-to-frequent neuritic plaques, and Braak stages V to VI neurofibrillary tangles (NFTs). Controls were clinically nondemented subjects with sparse or no neuritic plaques and NFTs less than or equal to Braak stage II. The AD patients and controls with Lewy body disease involving the brainstem (including substantia nigra), amygdala, middle frontal gyrus, and patients with vascular brain disease manifested by grossly observed arterial territorial infarcts, grossly observed lacunar infarcts, or microvascular infarcts were excluded. Parkinson disease (PD) patients had the expected clinical signs, symptoms, and midbrain—but not cerebral cortex—Lewy body pathology.

ELISAs

Brain samples were homogenized, sequentially extracted in 10 mmol/L Tris, 1 mmol/L ethylene glycol tetraacetic acid, 1 mmol/L dithiothreitol, 10% sucrose, and then extracted 3× with 1% Triton X-100, as previously described (19). Remaining detergent-insoluble material was extracted with 70% formic acid. Formic acid extracts of detergent-insoluble proteins were resolubilized and adsorbed onto 96-well plates as described elsewhere (19). The EAAT2/GLT-1 was detected with antibodies AB12 and GLT-1A (20). Presenilin-1 (PS1) was detected with PS1 N-terminal fragment antisera (21). Amyloid-β was detected with 4G8 (Covance/Signet Laboratories, Dedham, MA). Total tau was detected using anti-tau antibody (Dako, Carpinteria, CA). The ELISA plates were developed using standard methods with horseradish peroxidase–conjugated antibodies and tetramethylbenzidine substrate.

Immunohistochemistry and Biochemistry

Standard immunohistochemical methods were used to evaluate EAAT2 staining in paraffin-embedded postmortem brain sections. Slides were incubated with AB12 and developed using 3,3′-diaminobenzidine (Vector Laboratories, Burlingame, CA). Double immunostaining labeled EAAT2 (DAB brown chromogen) and either total tau ([Tau-2] Sigma, St Louis, MO) or Ab (4G8) labeled with Vector Red (Vector Laboratories). Counterstains were omitted in double label experiments. A Nikon Optiphot-2 microscope/Insight QE digital camera was used. Image acquisition was performed using Spot imaging software (Diagnostics Instruments, Sterling Heights, MI) and formatted with Photoshop. For each experiment, images were acquired and digitally processed under identical conditions. Digital image processing was limited to linear brightness and contrast adjustments, which were performed identically on experimental and control images.

Mouse brain extracts were solubilized in Laemmli sample buffer. Total Triton X-100–soluble protein concentrations were determined by the BCA method (Pierce, Rockford, IL) and Western blotted with AB12 or GLT-1A and detected using horseradish peroxidase–conjugated antibodies and chemiluminescence.

TABLE. Patient Demographic and Pathological Characteristics

Group	n	M/F	Age, years	PMI, hours	CERAD Score	Braak Stage
Hippocampus						
AD	22	6:5	84.3 ± 2.2	11.4 ± 1.4	Frequent (moderate–frequent)	VI (V–VI)
CDR = 0.5	14	7:8	88.9 ± 2.2	13.0 ± 2.0	Sparse (none–frequent)	IV (I–VI)
Norm	13	8:5	87.0 ± 1.7	9.8 ± 1.3	Sparse (none–sparse)	II (I–III)
PD	4	1:1	81.0 ± 5.7	17.8 ± 2.2	Sparse (none–sparse)	II (II–III)
Frontal cortex						
AD	55	6:5	82.7 ± 1.3	11.6 ± 0.8	Frequent (sparse–frequent)	VI (V–VI)
CDR = 0.5	23	1:1	90.4 ± 1.8	12.5 ± 1.4	Sparse (none–frequent)	III (I–VI)
Norm	20	2:3	90.1 ± 1.7	11.2 ± 1.2	None (non–sparse)	II (I–III)
PD	4	3:1	84.9 ± 3.7	10.5 ± 4.3	None (none–sparse)	II (I–III)

AD, Alzheimer disease; CDR, Clinical Dementia Rating; Norm, normal controls; PD, Parkinson disease; M/F, male-female ratio; Age, age at death; PMI, postmortem interval; CERAD, Consortium to Establish a Registry for Alzheimer Disease.

Liquid Chromatography-Tandem Mass Spectrometry

Equal amounts of formic acid–extracted protein were prepared from 5 AD subjects (mean age, 80 years; 3 women and 2 men; Consortium to Establish a Registry for Alzheimer Disease [CERAD] neuropsychological battery score, moderate or frequent; Braak stage VI), pooled, dried, dissolved in bicarbonate buffer, reduced, and treated with iodoacetamide before being subjected to trypsin digestion, as previously described (22). Eluted peptides were resuspended in 0.1% formic acid, separated by 2-dimensional microcapillary high-performance liquid chromatography, and amino acid sequences of separated peptides were determined by tandem mass spectrometry (ThermoFinnigan, San Jose, CA). Proteins from the mixture were identified automatically using the SEQUEST program, which searched spectral data against the International Protein Database. Sensitivity and specificity of protein identifications were determined by PeptideProphet and ProteinProphet as previously described (22).

Statistics

Data were analyzed with analysis of variance, Pearson correlation tests, and Fisher exact tests using SPSS 15.0 (SPSS, Chicago, IL). We predicted that detergent-insoluble EAAT2 would be highest in later-stage AD cases, lower in cases with a CDR = 0.5, and lowest in normal controls and PD patients lacking concurrent AD pathology. To test specifically this a priori prediction, well-established analysis of variance trend analyses methods (23, 24) were used with the trend weights −2, −2, 1, and 3 corresponding to the PD, normal controls, CDR = 0.5, and AD groups, respectively. In keeping with accepted methods, these trend weights were selected because they are orthogonal integers (sum to 0) and represent the originally predicted relationships among the study groups (23, 24). Specifically, we predicted that the levels of insoluble EAAT2 in the PD and normal control groups would be both comparable to each other and lower than the other 2 groups (−2, −2 for PD and normal controls, respectively). The insoluble EAAT2 levels of the CDR = 0.5 group were predicted to be higher than PD and normal controls but lower than the AD group, whereas the AD group was expected to have the highest insoluble EAAT2 levels (+1, +3 for the CDR = 0.5 and AD groups, respectively). These trend analyses followed only statistically significant omnibus analysis of variance results. Because this was the only trend predicted a priori, no other trend analysis was attempted.

RESULTS

Case Material

Among the hippocampal sample AD, CDR = 0.5 (intended to approximate mild cognitive impairment [MCI]), normal control, and PD subject groups studied, differences in male-female ratios, postmortem intervals, and ages at death were not statistically significant (Fisher exact tests [9] = 0.993, $F_{3,49} = 1.770$, and $F_{3,49} = 1.149$, respectively). Group differences in CERAD scores and Braak stages were significant (Fisher exact tests [9] = 46.385, $p < 0.00001$; $F_{18} = 71.067$, $p < 0.00001$, respectively). For the frontal cortex subject sample group, differences in the male-female ratios and postmortem intervals were not significant (Fisher exact tests [3] = 2.646 and $F_{3,98} = 0.245$, respectively). Ages at death were statistically significant ($F_{3,98} = 5.708$, $p < 0.001$) because primarily of the AD patients who tended to die earlier than other subjects. As expected, CERAD scores and Braak stages were statistically significant among the groups (Fisher exact test [9] = 87.238, $p < 0.00001$; $F_{18} = 115.049$, $p < 0.00001$, respectively) (Table).

Detection of Detergent-Insoluble EAAT2 in AD by Mass Spectrometry

To examine whether detergent-insoluble EAAT2 accumulates in AD, we performed mass spectrometry on tryptic digests of total detergent-insoluble proteins pooled from 5 autopsy-confirmed AD patients. A total of 348 statistically significant ($p < 0.05$) sequence-to-spectra matches corresponding to EAAT2 tryptic peptide fragments were identified (Fig. 1A). These fragments clustered in 6 primary domains located throughout EAAT2 (Fig. 1B), suggesting that the entire molecule was represented in the detergent-insoluble protein fractions.

These data confirm that Triton X-100–insoluble EAAT2 is present in the brains of AD patients. Despite the structural accuracy of liquid chromatography tandem mass spectrometry, this approach is not well suited for quantitative comparisons between affected and control subjects. To examine

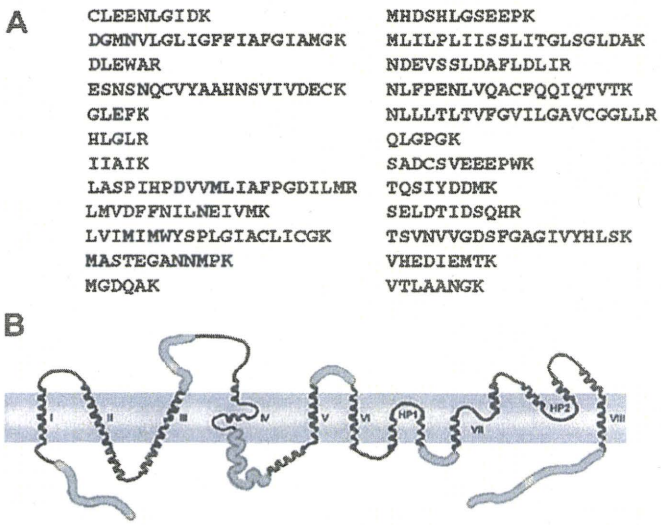

FIGURE 1. Detergent-insoluble excitatory amino acid transporter 2 (EAAT2) is present in Alzheimer disease (AD) frontal cortex. **(A)** A total of 348 EAAT2 tryptic fragments identified by liquid chromatography tandem mass spectrometry performed on Triton X-100–insoluble proteins from 5 AD patient cerebral cortex samples corresponded to the 24 unique EAAT2 sequences shown. **(B)** The EAAT2 tryptic fragments mapped to 6 primary structural regions indicated by gray highlighting located throughout the molecule. This EAAT2 model was modified from x-ray crystal structure results of Yernool et al (25). The primary transmembrane domains are indicated (I–VIII). Hairpin structures denoted as HP1 and HP2 form the glutamate-binding/gating domain.

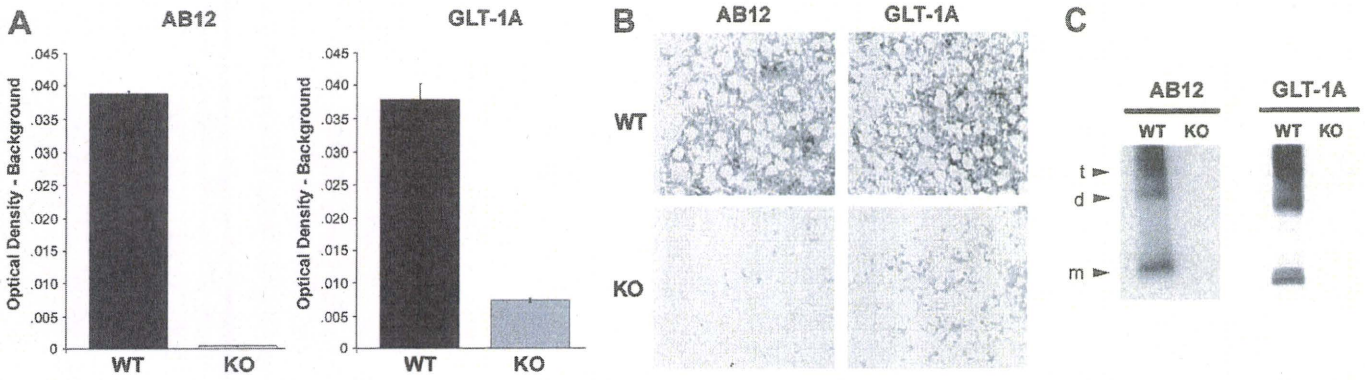

FIGURE 2. Specificity of excitatory amino acid transporter 2 (EAAT2) detection. Two different anti-EAAT2 antibodies (AB12 and GLT-1A that recognize the N- and C-terminal, respectively) were used. Pan-specific AB12 recognizes all EAAT2/GLT-1 isoforms; GLT-1A recognizes EAAT2a/GLT-1a, the most abundant EAAT2 isoform in cortex and hippocampus. Using brain tissue from GLT-1 wild-type (WT) and knockout (KO) mouse ELISAs **(A)**, immunohistochemistry in cortex **(B)** and Western blots **(C)** prove the specificity of EAAT2/GLT-1 detection. The EAAT2/GLT-1 is a homotrimer that resolves as monomers (m), dimers (d), and apparent trimers (t) with approximate molecular weights of 70 kd, 150 kd, and more than 200 kd, respectively. Error bars in **(A)** indicate SEM of WT and KO brain tissue samples measured in triplicate.

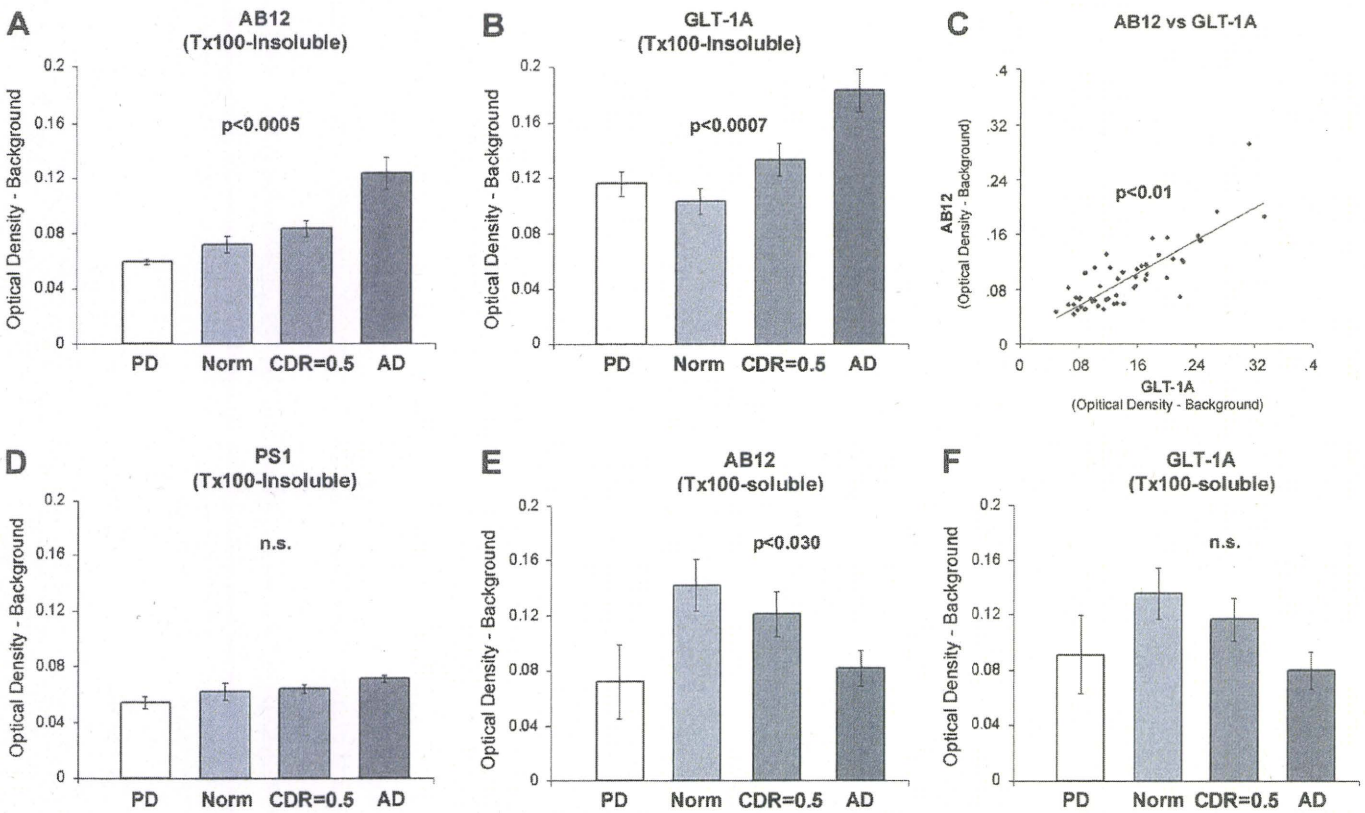

FIGURE 3. Detergent-insoluble excitatory amino acid transporter 2 (EAAT2) levels were increased in hippocampi of patients with Alzheimer disease (AD) pathology. **(A)** Total Triton X-100–insoluble proteins from Parkinson disease (PD, n = 4), normal control (Norm, n = 13), mild cognitive impairment (n = 14), and later-stage AD (n = 22) patients were solubilized with formic acid and analyzed by AB12 ELISAs to quantify detergent-insoluble EAAT2 levels. **(B)** Total Triton X-100–insoluble EAAT2 levels were measured by GLT-1A ELISAs as in **(A)**. **(C)** Scatter plot shows a correlation between insoluble EAAT2 levels measured by AB12 and GLT-1A ELISAs for all subjects (n = 53). The p value indicates statistical significance determined by Pearson correlation. **(D)** Total Triton X-100–insoluble levels of presenilin-1 (PS1) were measured in the same samples as shown in (**A** and **B**). **(E, F)** Triton X-100–soluble EAAT2 levels from same samples as in (**A, B,** and **D**) were measured by AB12 and GLT-1A ELISAs, respectively. The p values **(A, B, D–F)** indicate results of overall single-factor analysis of variance. CDR, Clinical Dementia Rating; n.s., not significant.